

MASTER

Light emission from quasi 2D layered perovskites

Croes, G.T.C.

Award date:
2018

[Link to publication](#)

Disclaimer

This document contains a student thesis (bachelor's or master's), as authored by a student at Eindhoven University of Technology. Student theses are made available in the TU/e repository upon obtaining the required degree. The grade received is not published on the document as presented in the repository. The required complexity or quality of research of student theses may vary by program, and the required minimum study period may vary in duration.

General rights

Copyright and moral rights for the publications made accessible in the public portal are retained by the authors and/or other copyright owners and it is a condition of accessing publications that users recognise and abide by the legal requirements associated with these rights.

- Users may download and print one copy of any publication from the public portal for the purpose of private study or research.
- You may not further distribute the material or use it for any profit-making activity or commercial gain

Light emission from Quasi 2D Layered Perovskites

Master thesis

Guillaume Croes

Supervisors:
prof. dr. R. Coehoorn
prof. dr. J. Genoe

Eindhoven, October 2018

Preface

This thesis is the result of a twelve month internship at the Large Area Electronics (LAE) department at IMEC (Interuniversitair Micro-Elektronica Centrum) in Leuven, Belgium. Founded in 1984, IMEC is now the largest independent research center in Europe with about 4000 employees. IMEC's original focus was directed towards micro- and nano-electronics. However, over the years it branched out in various scientific fields and locations all over the world. Although its heart and lungs are still nanoelectronic related research many other topics are nowadays looked into. LAE is a good example of this, as they work around thin film displays, sensors and integrated circuits. One of the newer topics in the research group is perovskite light emitters which also is the topic of this thesis.

Contents

Contents	iv
1 Introduction	1
1.1 Perovskites	1
1.2 Motivation for Perovskites LEDs	3
1.3 State of the art	5
1.3.1 History of perovskite light emitting diodes	5
1.3.2 Abnormal perovskite behaviour	7
1.4 Goal of the thesis	14
1.5 Approach	14
2 Fabrication Technique and Measurement Setup	16
2.1 Precursor solution preparation	16
2.1.1 Poly-TPD	16
2.1.2 Perovskite	16
2.2 Device fabrication	18
2.3 Measurement setup	19
2.3.1 Calculating external quantum efficiency	20
2.3.2 Calibration	22
3 Results and Discussion	23
3.1 Perovskite layer optimization	23
3.2 ETL alternatives	32
3.3 Emission zone	35
3.4 Peak Shift and prevention	36
3.4.1 Emission Peak Shift	36
3.4.2 Efficiency Increase	38
3.4.3 Preventing Ion movement	39
4 Summary, Conclusions and Outlook	41
Bibliography	43
A Scanning Electron Microscopy	48

Chapter 1

Introduction

In this chapter a general introduction is given to the topic of this thesis. First, some background is given to the employed materials and their various crystal structures. This thesis is focused around infrared lighting and thus all the mentioned materials here are specifically chosen for that application. Next, a motivation is given to why this research is interesting based on some excellent properties perovskites have shown. The history of perovskite light emitting diodes and several reported abnormal phenomenon are addressed. Finally, the goal of this thesis is explained followed by the approach that was taken.

1.1 Perovskites

In the last decade, hybrid organic/inorganic perovskites have become a hot topic primarily due to solar cell research where they are considered as candidate to achieve low cost and high efficiency photovoltaics. More recently these interesting materials have started to branch out into other fields such as photodetectors and light emitting diodes (LEDs). The name "perovskite" was originally solely used for a mineral composed of calcium titanate (CaTiO_3) which got its name after the Russian minearologist Lev Perovski. However, nowadays it refers to materials having the same crystal structure as the calcium titanate mineral.

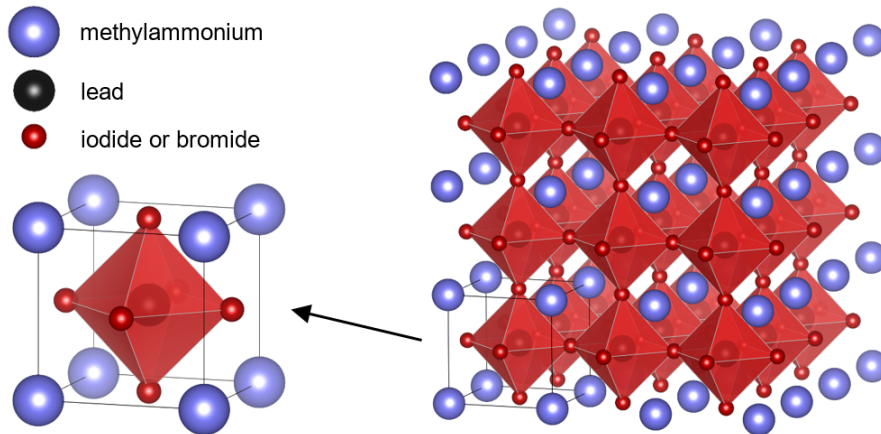


Figure 1.1: Schematic of a perovskite crystal structure and unit cell indicating the staple materials used in this thesis. Here, lead is represented by the black center spheres, the halide component is indicated with the red spheres forming an octahedron and methylammonium is represented by the blue spheres forming a cube.

The interest in these materials is mainly fueled by their excellent properties such as a direct tunable bandgap, high ambipolar charge mobilities and low temperature processing. A more accurate name for the currently used materials is organic/inorganic halide perovskites, since they consist of organic molecules or alkali metals, transition metals and halides. Their general structure is often written as ABX_3 in which A is an organic molecule or alkali metal, B is a divalent transition metal and X is a halide anion. In general, the structure is quite flexible so that a wide range of constituents will still result in good crystallinity as long as their radii fit in the structure made by the other constituents. The more common materials for A are methylammonium ($CH_3NH_3^+$), formamidinium ($NH_2CH=NH_2^+$) and cesium (Cs^+), B is often lead (Pb^{2+}), copper (Cu^{2+}) or tin (Sn^{2+}) and X is commonly iodide (I^-), bromide (Br^-) or chloride (Cl^-). Here methylammonium lead iodide bromide ($MAPbI_{3-x}Br_x$) is used as building block to base further development on. In this specific case the unit cell has a lead atom as center which is surrounded by six halide atoms forming an octahedron. Additionally the methylammonium atoms form a cube while the halide atoms lie in its planes as can be seen in Figure 1.1 The crystal structure has several phases which are temperature dependent. The most common ones are cubic, orthorhombic and tetragonal. [1].

One interesting way to tune perovskites is by using large organic cations instead of the normal constituent in the A position. A carefully chosen cation, in this case butylammonium, will break up the individual perovskite layers and form a spacing layer between them, creating a layered two dimensional structure. Further tuning can be achieved by only partially replacing them, resulting in a mixture between normal perovskite and a layered structure. Instead of single perovskite layers the material will now have several grouped together, separated from each other by a spacing layer.

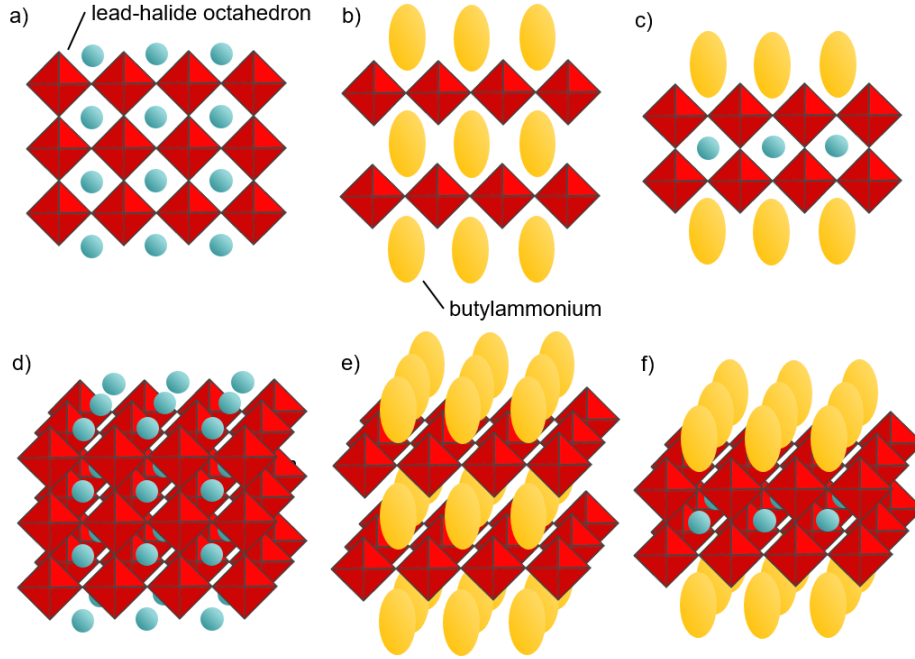


Figure 1.2: Schematics comparing the build up of various perovskite crystal structures. To simplify the halide octahedrons have been made solid and both 2D and 3D versions of the structures are shown. Schematic d), e) and f) show 3D versions of respectively a), b) and c). a) A normal 3 dimensional perovskite or a Ruddlesden-Popper phase perovskite of order infinity. ($n = \infty$) b) A pure 2 dimensional perovskite lattice or Ruddlesden-Popper perovskite with phase $n = 1$. The small organic cations are replaced by larger organic cations to separate individual perovskite layers from each other. c) A quasi 2 dimensional perovskite lattice or Ruddlesden-Popper perovskite with phase $n = 2$. Both large and smaller organic cations are present in the perovskite.

Figure 1.2 shows a comparison between each structure and indicates the materials of choice. Each structure is shown twice, once in a simplified version and once in 3D. To further simplify the schematics the halide octahedra have been made solid. The materials are often called Ruddlesden-Popper phase perovskites and generally are denoted with an order indicating the amount of normal layers between each spacing layer. A material only having large cations will thus be denoted as being of order one ($n = 1$) while normal bulk perovskite can be viewed as being of order infinity ($n = \infty$). On top of that, materials in-between both extremes are often denoted as quasi 2D perovskites.

1.2 Motivation for Perovskites LEDs

Light emitting diodes are becoming omnipresent in everyday life, with their applications ranging from normal everyday lighting to displays and signaling. Their main advantages over other light sources are their efficiency and durability as well as the wide range of colours that can be emitted. LEDs operate due to electroluminescence i.e. the radiative recombination of electrons and electron holes due to an applied bias to a device or material. This effect was discovered by H. J. Round in 1907 while working at Marconi Labs. One of the first somewhat practical LEDs became available in the sixties, when in 1968 Monsanto started mass producing red emitting LEDs made from gallium arsenide phosphide (GaAsP). They were primarily used as indicators in seven digit displays for calculators and alarm clocks. However they did not emit enough light so that they could be used for everyday lighting applications. Since then, LEDs have been steadily improving in light output, nowadays LEDs easily attain a luminous efficacy (lm/W) of more than a hundred while incandescent light bulbs reach a value of about 15 lm/W. Additionally various scientific fields have sprouted from the LED advancements. For example the use of organic materials lead to research into organic light emitting diodes (OLEDs) which are now the best technology available for smartphones and other displays.

A typical perovskite LED differs from the standard pn junction based LED as can be found in an inorganic LED or transistor, instead it consists of an intrinsic perovskite layer sandwiched between a hole transport layer (HTL) and an electron transport layer (ETL). Additionally there are contacts and charge injection layers (EIL and HIL) on both sides. The contacts supply charges to the LED and the injection layers make sure that this charge optimally reaches the transport layers. A schematic of such a structure can be seen in Figure 1.3. Next to good transport properties for either electrons or holes the transport layers also function as blocking layers for holes and electrons respectively. This creates what are called selective contacts, which means that they only let one type of charge carrier pass. Charge carriers thus become confined to the perovskite layer, which will ensure that they have a high chance of giving a radiative recombination.

Light emitting diodes based on perovskites are a topic gaining a lot of traction in the LED field, driven by promising properties such as long electron and hole diffusion lengths and a low nonradioactive recombination rate. [2] They offer a pathway to achieve low cost highly efficient light emitters. [3] Initial results also show that they are a candidate to achieve bright emission at high current densities without substantial efficiency roll-off. [4] Another benefit of perovskites is the flexible crystal composition so that their emission spectrum can be tuned over the entire visible light spectrum. Depending on the halide component being iodide, bromide or chloride bandgaps of about 1.5, 2.2 and 3.1 eV or emission wavelengths of 825, 565 and 400 nm respectively can be created. Additionally, mixed halide perovskites allow these values to be tuned to any value in between so that the entire visible range can be emitted. On top of that amplified spontaneous emission has been observed, opening up the possibility towards thin film lasing. [5] [6]

Depending on the type of application different types of LEDs are favoured. Common criteria to determine the most suited LED are their lifetime, efficiency and size. For example, LEDs used for everyday lighting are mostly of inorganic nature and thus quite bulky whereas LED displays

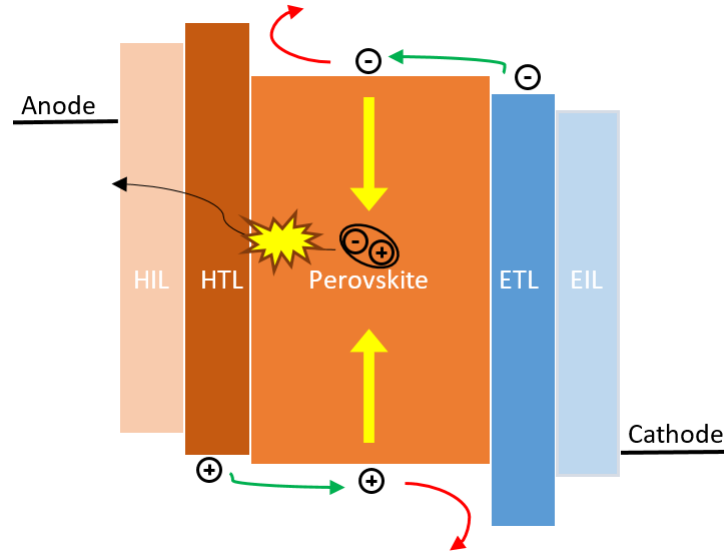


Figure 1.3: Schematic of an ideal PeLED structure. Selective contacts are employed to inject and confine charge carriers supplied from the contacts to the emissive perovskite layer where they recombine radiatively.

are made from organic semiconductors. These materials are low-cost and can be processed as thin film making them ideal for an application where resolution is an important factor. Since perovskites are also a thin film technology it makes them a competitor to OLEDs and quantum dots (QDs). Although OLEDs outclass their competition in stability and efficiency, they still have some intrinsic problems. This could make perovskites a clearly better option in the future in some specific situations. For example, OLEDs suffer from an effect called efficiency roll-off which becomes apparent at high current densities, where the efficiency of a device will start to drop significantly resulting in a lower percentage of radiative recombinations. This inherently makes OLEDs an impractical solution for applications requiring high brightness such as lasers and certain enhanced reality applications. Perovskites could be a solution to this problem as the loss mechanisms causing the efficiency roll off might function completely differently.

Another intrinsic problem OLEDs suffer from depends on their physical emission mechanism. In general electrons and holes will form an exciton before recombining decreasing their energy. However two different types of excitons are formed, called singlet and triplet excitons. The problem here lies with the triplet excitons which intrinsically cannot recombine radiatively. Unfortunately, quantum mechanics dictates that 75 % of all the formed excitons are triplet excitons. In a perfect OLED the maximum internal quantum efficiency (IQE) would be only 25 %. To circumvent this problem phosphorescent dopants are added into the emissive layer, which often contain a heavy metal to cause some triplet excitons to become singlet excitons due to a strong spin-orbit coupling. As a result, they can dramatically increase the efficiency of OLEDs. In perovskites this effect might not be a problem, as bright triplet exciton emission has been reported. [7]

Additionally, perovskites are reported to have a high colour purity with emission widths as small as 20 nm. An industrial standard OLED and inorganic quantum dots, however both have a broader full width at half maximum (FWHM) of 40 nm and 30 nm respectively. [8] [9] [10] [11] [12] Figure 1.4 shows how the spectra would compare to each other assuming that the emission can be represented by a Gaussian. This property is important for light emitting applications working at the edges of the visible spectrum. A very sharp peak can reach this edge with only a minimal part of it in the non visible range and thus loses as little energy as possible. For broader emission

spectra the emission wavelength is often chosen sufficiently far from the edge and hence some of the visible light range is lost.

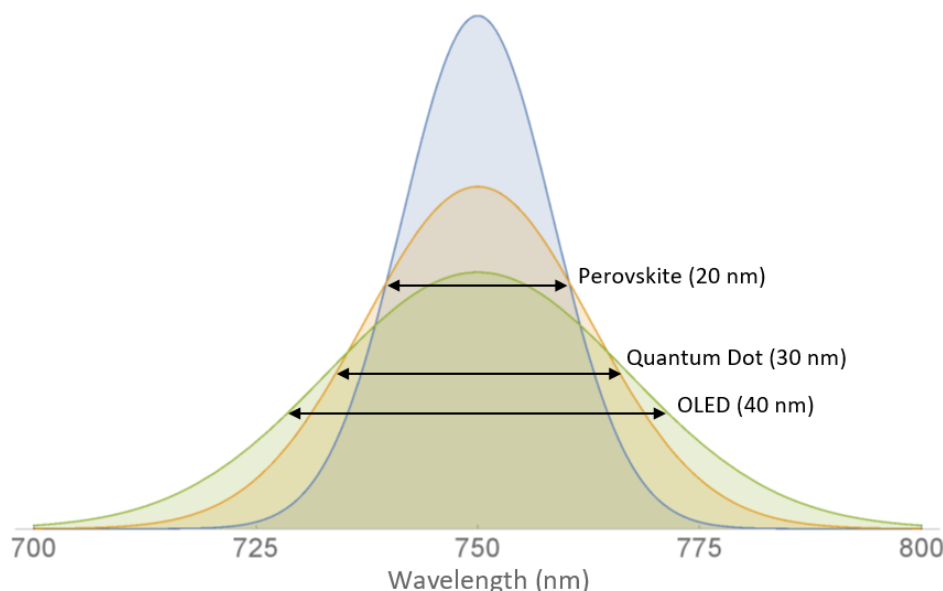


Figure 1.4: Schematic comparing the FWHM of common light emitters assuming their emission spectra have a Gaussian distribution. Since Gaussian distributions have the same area under each curve this illustrates the superior colour purity of perovskites as light emitters

Even though perovskites show very promising properties several things still require some innovation. Remarkable high external quantum efficiencies (EQE) reaching above 14 % have been achieved with Ruddlesden-Popper phase perovskites, however still more research is needed to push these values closer to those of commercial LEDs. On top of that, a recurring problem for PeLEDs is their stability. At the moment, devices only reach hour-long stabilities which is insufficient for real-world applications. Further work into intrinsic stabilization and the prevention of degradation from outside influences such as water and air or unbalanced charge injection and joule heating is needed. Another major concern is the toxicity of the employed materials since the best results so far have been achieved with lead based perovskites. New efforts should be made to find and optimize replacements such as tin and copper to make these devices safe for the environment and ourselves.

1.3 State of the art

1.3.1 History of perovskite light emitting diodes

Low temperature PeLEDs

Organic/inorganic hybrid perovskite LEDs were first reported in 1994 when $(\text{C}_6\text{H}_5\text{C}_2\text{H}_4\text{NH}_3)_2\text{PbI}_4$ was used as emitter. [13] The device operated at the temperature of liquid nitrogen and emitted at around 520 nm and a narrow FWHM of 10 nm. A luminance of more than $10 \times 10^3 \text{ cdm}^{-2}$ was achieved at a current density of 200 Am^{-2} . No major breakthroughs in PeLED research were achieved until 2014 when perovskites had emerged as excellent light absorbers for photovoltaics.

Room temperature PeLEDs

The first room temperature PeLED reached an efficiency of 0.76 % and 0.1 % for infrared and green emitters respectively by employing a thin perovskite layer to spatially confine the charge carriers for bimolecular recombination. The infrared LED was made by stacking indium tin oxide (ITO)/ titanium dioxide (TiO_2)/ $\text{CH}_3\text{NH}_3\text{PbBr}_{3-x}\text{Cl}_x$ / poly(9,9-dioctylfluorene) (F8)/ molybdenum oxide (MoO_x)/ silver (Ag) on top of each other and reached a radiance of $13.2 \text{ W sr}^{-1}\text{m}^{-2}$ at a current density of about $3.6 \times 10^3 \text{ Am}^{-2}$. The green device stack was build up of indium tin oxide (ITO)/ poly(3,4-ethylene dioxythiophene):poly(styrenesulfonate) (PEDOT:PSS)/ $\text{CH}_3\text{NH}_3\text{PbBr}_3$ / F8/ calcium (Ca)/ Ag. A luminance of 364 cd m^{-2} was reached at a current density of $12.3 \times 10^2 \text{ Am}^{-2}$. The best efficiency with a similar perovskite layer was achieved a year later and reached an EQE of 3.5 and 0.8 % for near-infrared and green emitters respectively. The key to the high device efficiency was the interface between the oxide electron transporting layer and the emissive perovskite layer. To improve the surface wetting a thin layer of polyethyleneimine (PEI) was deposited on the zinc oxide (ZnO), this additional layer decreased the static contact angles of water on the ZnO from 53° to 27° . The surface thus became more hydrophilic and dewetting was suppressed resulting in excellent crystalline three-dimensional perovskite. Their employed device structure consists of indium tin oxide (ITO), PEI-modified ZnO, Perovskite, poly(9,9-dioctyl-fluorene-co-N-(4-butylphenyl)diphenylamine) (TFB), molybdenum oxide (MoO_x) and gold (Au) where the perovskite is either $\text{CH}_3\text{NH}_3\text{PbI}_{3-x}\text{Cl}_x$ or $\text{CH}_3\text{NH}_3\text{PbBr}_3$ for infrared and green emitters respectively. Interesting to note is that with this structure the green emitting devices reached a luminance of more than $20 \times 10^3 \text{ cdm}^{-2}$. The difference in EQE between the two types of perovskite is likely caused by less complete coverage leading to more pinholes. [14]

At this point, it became clear that perovskite had an intrinsic property that was stopping them from being more efficient. The low exciton energy (E_b) was identified as a possible bottleneck. In the case of $\text{CH}_3\text{NH}_3\text{PbI}_3$, E_b is about 16 meV at low temperature and only a few millielectronvolts at room temperature. [15] Thus E_b falls below the available thermal energy ($E_T = k_b T \approx 25 \text{ meV}$) which leads to immediate dissociation into free charge carriers of any formed excitons. Fortunately, the exciton binding energy can be increased by using Ruddlesden-Popper phase perovskites which form quantum well like structures. One difficulty with this method is that the separation between individual perovskite layers by large cations reduces the charge carrier mobility. Alternatively, higher efficiencies can be achieved by decreasing the crystallite size or reducing the layer thickness which makes it more likely that opposite carriers find each other by confining them.

Nanograin PeLEDs

An early adaptation of one of these techniques was to use spatial confinement in a nanograin perovskite. This approach led to green emitting devices with an EQE of about 8.5 % reaching a luminance of almost $17 \times 10^3 \text{ cdm}^{-2}$. It was achieved by fine stoichiometry control and nanograin engineering by nanocrystal pinning or NCP. First and foremost, exact stoichiometric control was needed to prevent metallic lead atoms from being present in the perovskite layer, as these excess atoms increase the nonradiative decay rate. Secondly, the reduction of the grain-size in the perovskite film gives improved uniformity, coverage and radiative recombination. The smaller grainsize confines the excitons and leads to smaller exciton diffusion lengths as well as longer exciton lifetimes. The employed device structure was a glass substrate covered with a self-organized conducting polymer (SOCp), $\text{CH}_3\text{NH}_3\text{PbBr}_3$, 2,2,2-(1,3,5-benzinetriyl)-tris (1-phenyl-1-H-benzimidazole) (TPBi), lithium fluoride (LiF) and aluminium (Al). An important principle during the NCP was that the antisolvent already contained TPBi, resulting in a nanograin perovskite layer with a TPBi layer on top. [16]

Ruddlesden-Popper phase PeLEDs

So far the best results in the field of perovskite light emitting diodes have been achieved by employing Ruddlesden-Popper phase perovskites. By incorporating the right amount of large cations the optimal spot between conductivity and confinement in the perovskite layer could be found. The best result for a green emitter has been achieved with a phenylethylammonium ($\text{C}_6\text{H}_5\text{C}_2\text{H}_4\text{NH}_3^+$, PEA), formamidinium bromide ($\text{HC}(\text{NH}_2)\text{Br}$, FABr) and lead bromide (PbBr_2) based perovskite reaching an EQE of 14.36 %. The used device stack consists of ITO/PEDOT:PSS/PEA₂(FAPbBr₃)_{*n*-1}PbBr₄/TPBi/LiF/Al. The key to achieving high EQE values was composition and phase engineering together with surface passivation of the perovskite. The small molecule trioctylphosphine oxide was spincoated on top of the perovskite layer as passivation layer. An increase in the photoluminescence quantum yield and the fluorescence lifetime was observed as result. [17]

For the moment the best result for a red-infrared emitter has been achieved with a 1-naphthylmethylamine iodide, formamidinium iodide and lead iodide (PbI_2) based perovskite reaching an EQE of 12.7% and sustaining EQEs of approximately 10% at high current densities up to $5 \times 10^3 \text{ Am}^{-2}$. The used device stack consisted of ITO, PEI-modified ZnO, perovskite, TFB, MoO₃ and Au. The key to achieving high EQE values together with a reduced efficiency roll-off was finding the cause of the efficiency roll-off and preventing it. By performing simultaneous EL and PL measurements, luminescence quenching likely caused by non-radiative Auger recombinations was found to be the main cause of the efficiency roll-off. Auger recombination occurs when an electron recombines with a hole but instead of emitting a photon the energy is given to an extra electron. This electron will then lose the energy to thermal vibrations. Since three charges carriers are required this effect only plays a major role at high charge carrier densities. One way to reduce this effect is to decrease the local carrier density in the quantum wells which can be achieved by increasing their size. The optimized devices are thus slightly more 3D which reduces non-radiative recombinations. [4]

To accurately assess where the PeLEDs results stand, OLEDs are a good comparison. At the moment perovskites already reach equally high if not higher efficiencies than fluorescent OLEDs (FluOLEDs). Looking at FLuOLEDs with a similar planar structure, efficiencies up to 11.7 % and 10.9 % for green and red emitters respectively can be reached. Stability wise these devices drop 50 % in luminance after ~190 hours of constant biasing. [18] Alternatively, phosphorescent OLEDs (PhOLEDs) are superior in every aspect when compared to PeLEDs. They reach EQEs of 26 % and 26.1 % for green and red PhOLEDs respectively. [19] [20] On top of that, PhOLEDs are more stable than FluOLEDs are, lifetimes in the order of a million hours have been reported for red emitting LEDs. [21]

1.3.2 Abnormal perovskite behaviour

Research into perovskite solar cells has found that ionic migration occurs in perovskites to a certain extent. Due to the ionic nature of the perovskite lattice, the bonds are prone to breaking if sufficient energy is present. Once an atom breaks free it can migrate through the layer by jumping from vacancy to vacancy. The hopping is illustrated in Figure 1.6. Several theoretical studies have been performed for methylammonium lead iodide which estimate the activation energies of the ionic migration. The energies required to release an iodide, lead and methylammonium ion were found to be 0.58, 2.31 and 0.84 eV respectively by Eames et al. [22] Azpiroz et al. calculated the same values as 0.08, 0.80 and 0.46 eV and finally Haruyama et al. found activation energies of 0.32 eV for iodide and 0.57 eV for methylammonium. [23] [24] These values suggest that hybrid lead halide perovskites are mixed ionic-electronic conductors primarily due to iodide ions that require the least amount of energy to start migrating.

Next to the theoretical studies, ionic movement has also been observed experimentally. By

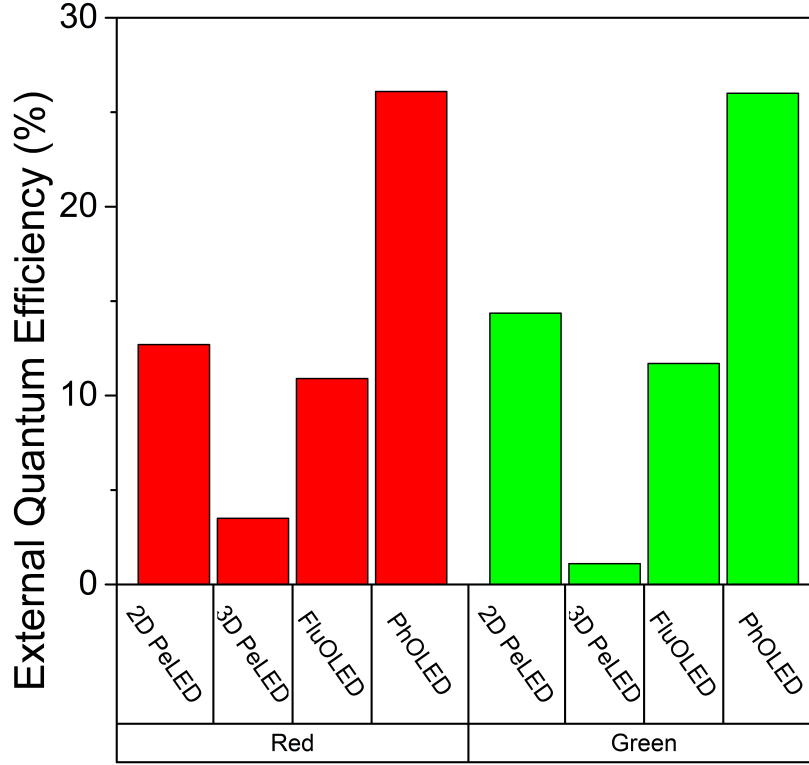


Figure 1.5: Comparison of the highest attained EQE by similar planar devices with different light emitting technologies. Both red and green light emitters are split up into 4 categories, namely 2D and 3D PeLEDs and fluorescent and phosphorescent OLEDs.

performing Galvanostatic direct current (DC) measurements on perovskite sandwiched between graphite electrodes mixed conducting behaviour could be revealed. The longer a current flows through this device the more ions accumulate forming an internal gradient. Simultaneously the voltage increases until it reaches a saturation value, in this steady state only electrons flow. On top of this the conductivities of ions and electrons could be determined giving $\sigma_e = 1.9 \times 10^9 \text{ Scm}^{-1}$ and an ionic conductivity of $\sigma_i = 7.7 \times 10^9 \text{ Scm}^{-1}$. [25]

In another work faradaic reaction cells were made to identify the major mobile ionic species. A current was applied to cells with the structure +Cu / MAPbI₃ / AgI / Ag-. The only observed phase change was that CuI had formed at the copper contact, indicating that only iodide transport is present in the perovskite. The same results were achieved when cells were made with a lead contact instead of copper. [26] Moreover this ion accumulation has been found to work as a form of capacitance. Since any applied current is shared between ionic and electronic conduction, ions such as iodide will start to migrate towards the interface of the perovskite and ETL. There they cannot pass any further and become trapped at the interface, this charge build up will continue until a new equilibrium forms. A similar effect was observed in films with laterally interdigitated electrodes with channel lengths of about 200 μm . Here PL measurements were performed as a function of time tracking the emission of the perovskite. A special setup was used that includes a microscope and wide field illumination together with a CCD camera to obtain PL images from large areas. This allows tracking of the PL intensity in time and space. Typical PL measurements on perovskites show dark areas, indicating non radiative recombination pathways. These are possibly caused by a high amount of defects associated with halide migration. Under a constant electric field the PL measurements show a bright PL front moving away from the cathode. [27]

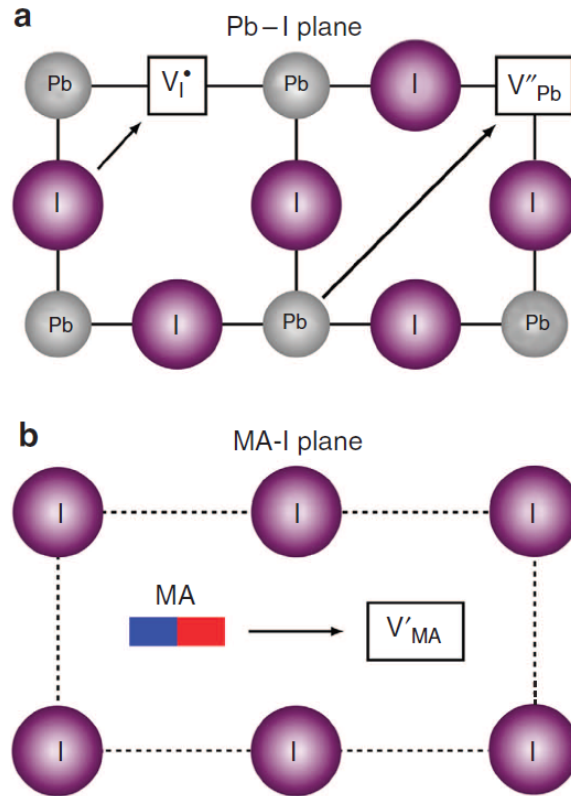


Figure 1.6: Schematic representation of the possible ionic transport mechanisms in methylammonium lead iodide if a vacancy were available. a) Illustration of the ionic hopping that iodide and lead would undertake if sufficient energy is supplied. b) Illustration of the migration mechanism for a methylammonium molecule. Graph taken from [22].

The exact implications of ion migration in hybrid lead halide perovskites are still being researched. However, more and more evidence links this phenomenon to perovskite phase separation, the anomalous hysteresis during $J(V)$ measurements and possibly also the efficiency increase during operation in PeLEDs.

Perovskite phase separation

Mixing halide components seems to be an easy and straightforward way to tune the perovskite bandgap. For the commonly used methylammonium lead halides combinations of iodide and bromide can be used to make materials with bandgaps ranging from 1.6 to 2.3 eV. This tuning seemed like an ideal way to achieve higher open circuit voltages in PSCs, however by increasing the bandgap i.e. by adding more bromide, the open circuit voltage did not increase by the expected amount and even decreased for large enough amounts of bromide. It turns out that this is caused by phase separation of the perovskite absorber.

The phase separation was found to be completely reversible and related to the light exposure of the solar cell. It was found experimentally that in the case of a mixed iodide and bromide perovskite the segregation leads to iodide rich domains ($\text{MAPb}(\text{I}_{0.8}\text{Br}_{0.2})_3$) and bromide rich domains ($\text{MAPb}(\text{I}_{0.3}\text{Br}_{0.7})_3$). [28] When the material reaches this state the cubic-to-tetragonal phase transition prevents further segregation. The effect was first observed during PL measurements where

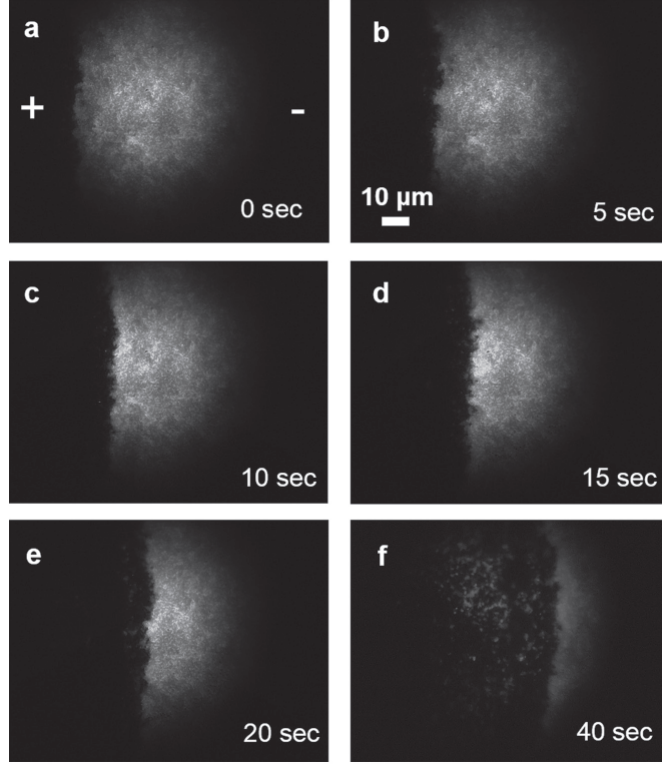


Figure 1.7: Time dependent PL measurements of a perovskite film under an electric field. A dark area forms at the cathode as time goes on due to iodide accumulation. Graph taken from [27].

samples where exposed to continuous illumination. After some time an additional peak at 1.68 eV appeared matching an iodide rich phase. Under continuous illumination this peak will grow in intensity until it reaches saturation. Figure 1.8 shows a simulation of ion movement and clustering matching well with experimental cathodoluminescence measurements. [29] Moreover, a similar effect also occurs in perovskites having a single halide component. By exposing the perovskite to light, a halide redistribution away from the illuminated area starts. Additionally, halide migration appears to be related to the reduction of fast non-radiative decay pathways and has been termed to be "cleaning" the perovskite layer. Again, this effect becomes most apparent during photoluminescence measurements where the PL intensity is monitored while it becomes higher due to the perovskite brightening. [30]

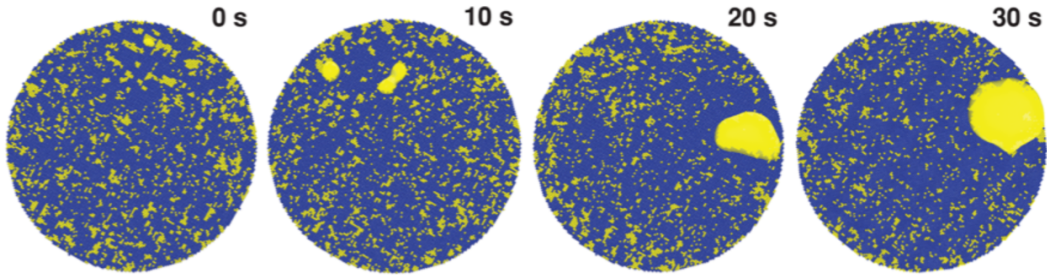


Figure 1.8: A series of snapshots of a simulation of ion movement showing iodide cluster formation. Yellow indicates iodide, blue indicate bromide. Graph taken from [29]

Physically the photoinduced phase segregation seems to be related to the gradient in carrier generation which depends on illumination wavelength and film thickness. One possible explanation states that the halide ions become more mobile due to the illumination which results in a net migration away from the illuminated surface. In mixed halide perovskites, the phase separation could be fueled by light absorption resulting in mobile ions together with ion specific mobilities. Here iodide ions could for example diffuse quickly out of an illuminated area while the less mobile bromide ions stay put. This would continue until a new equilibrium forms due to the net electric field that forms between the ion deficient illuminated area and its surroundings.

A possible consequence of the phase separation in mixed halide perovskite LEDs is that their peak emission wavelength can change during operation. Typical features of this phenomenon are a gradual approach towards a stabilized regime and relaxation towards the initial conditions after the bias is turned off. At this moment, no literature has really addressed the issue although its consequences can sporadically be found. A good example is Figure 1.9, here the emission spectrum is measured during consecutive $J(V)$ scans. The emission spectrum starts at 575 nm and slowly saturates towards 650 nm. [31]

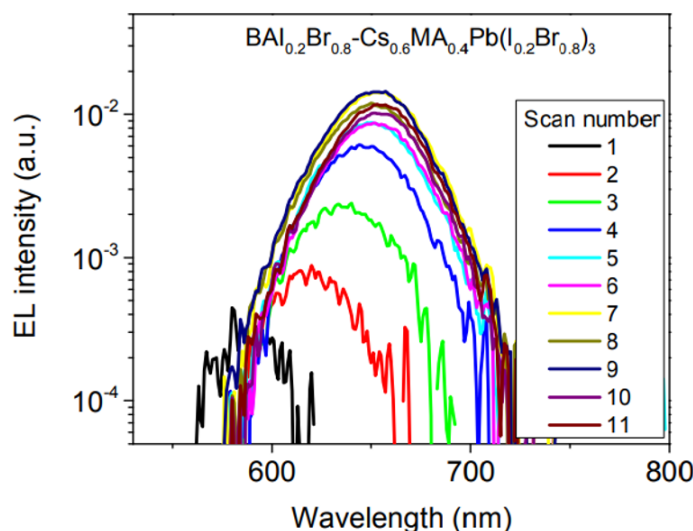


Figure 1.9: Change in the emission spectra of a PeLED measured during repeated IV scans on the same device. Graph taken from [31]

$J(V)$ Hysteresis

Quite early on in the perovskite solar cell research an interesting hysteresis behaviour was observed. This behaviour could be found in the $J(V)$ characteristic of perovskite solar cells and would be apparent as a difference between the forward and backward scan. The discrepancy between the two can be quite large and since $J(V)$ scans are used to determine the energy conversion efficiency, this also puts a question mark next to these values. [32]

The severity of the effect seems to depend on the device structure i.e. mesoporous versus planar devices, employed transport materials and prior biasing conditions. On top of that, it is strongly affected by the scan rate of an $J(V)$ measurement. Common scan rates for solar cells lie between 100 mV/s and 1 mV/s. It was found that the hysteresis is most apparent at intermediate scan rates and that it is not observed for extremely fast and slow scan rates.

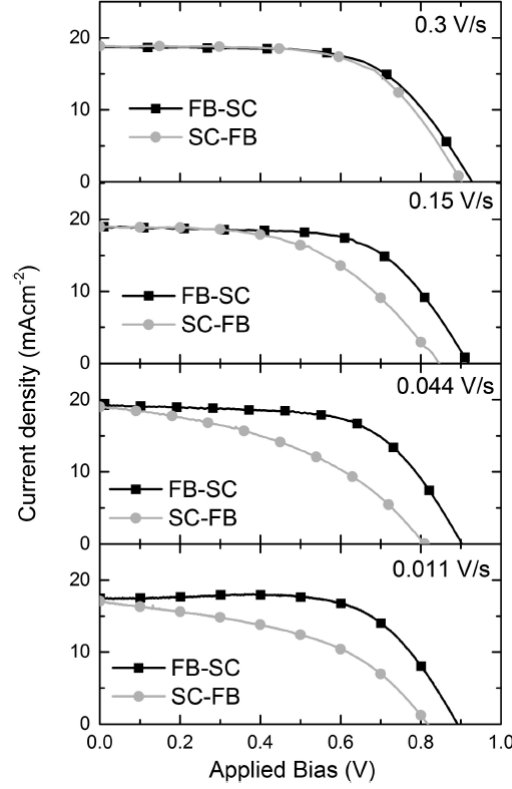


Figure 1.10: Current density versus voltage curves measured at different sweep rates showing various amount of hysteresis. FB and SC stand for forward bias and short circuit and indicate the direction of both scans. Graph taken from [32]

Many plausible explanations were put forward including mobile ions possibly acting as interstitial defects, high amounts of defects that act as trap states at the surface and ferroelectric polarization. Although no conclusive evidence has been found yet, most results tend to point in the direction of surface trap states related to ion movement in the perovskite film. This is because the hysteresis effect happens on a second timescale and the ferroelectric polarization occurs on much shorter timescales. [33]

If ion movement is the root cause, hysteresis can be explained by a capacitive effect. Under a forward scan (from short circuit to forward bias) the capacitance can be charged up due to the accumulating charges and the current through the diode is lower than expected. During a backward scan (from open circuit to short circuit) the opposite can happen where some of the stored capacitive charge can be extracted during the sweep. [34] [35] In impedance spectroscopy measurements the perovskite solar cells show a very high capacitance at very low frequencies which explains why low $J(V)$ scan speeds results in severe hysteresis. The same measurement also shows that at high enough frequencies the capacitance of the device starts to decrease hence why faster scan speeds do not show the hysteresis as prominent as slow scans. The effect is so detrimental for calculating precise conversion efficiencies that the steady state power output should be reported to make an accurate comparison together with the $J(V)$ curves.

Device efficiency increase

An increase in the device performance was recently found under the influence of electrical stress. [36] The EQE was found to increase from 5.9 % to 7.4 % while the PL intensity and time resolved decay lifetime increased indicating there is less nonradiative recombination. Figure 1.11 shows the device characteristics under subsequent electrical scans. The increase in EQE saturates after a certain amount of scans while simultaneously the $J(V)$ scans show an increase in slope in the zone around 2V. By looking at the diode equation trap assisted recombination seems to reduce as the ideality factor of the diode decreases. This factor is a term in the Shockley diode equation that states how much a real diode deviates from an ideal diode. In the ideal case it is equal to unity, however due to various kinds of recombinations the value can be higher.

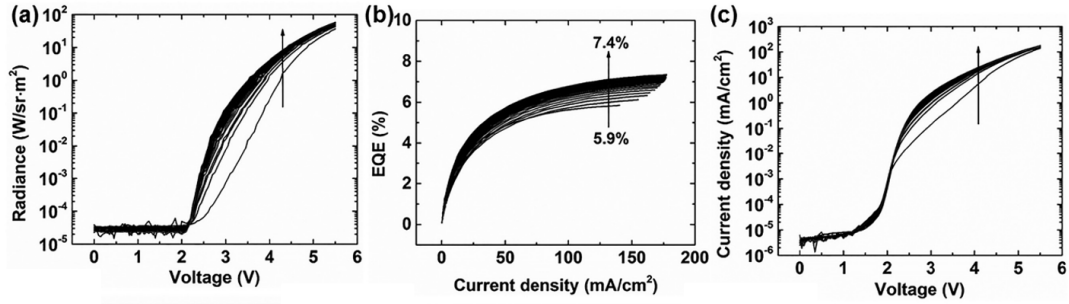


Figure 1.11: a) Radiance versus the applied voltage over the device. The subsequent sweeps result in an increasing radiance that saturates after some time. b) The external quantum efficiency during the subsequent scans, the efficiency increases from 5.9 % to 7.4 %. c) The $J(V)$ characteristics of a PeLED, the slope of the curve becomes increasingly steeper every subsequent scan. Graphs taken from [36]

To further understand the underlying mechanism temperature dependent measurements were performed. Again, devices were treated with several $J(V)$ scans while tracking the device characteristics but now at different temperatures. Figure 1.12, taken from [36] shows that at lower temperatures there is noticeable influence on the device efficiency. Slightly higher temperatures however do result in a strong increase in the efficiency. This seems to correlate with the $J(V)$ hysteresis which diminishes due to impeded ion movement at low temperature. [37] The most likely explanation is that ionic redistribution caused by the electrical stress fills vacancies and reduces interstitial defects. This will reduce the amount of trap-assisted nonradiative recombination and thus increases the EQE, PL intensity and PL lifetime.

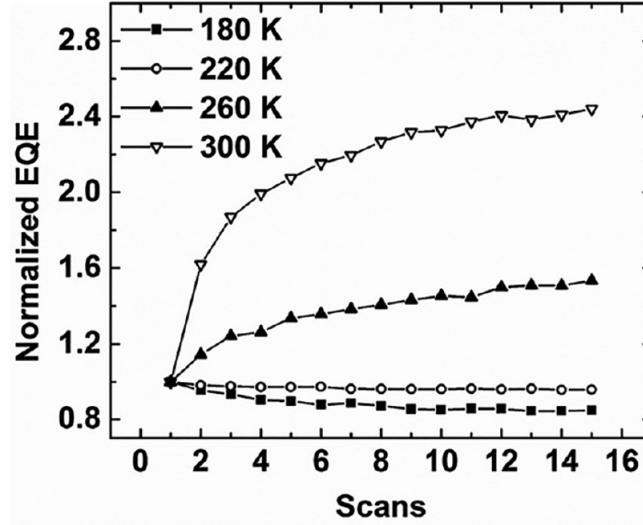


Figure 1.12: Temperature dependent tracking of the external quantum efficiency. An efficiency increase is only observed when sufficiently high temperatures are supplied. Graph taken from [36].

1.4 Goal of the thesis

Summarized, perovskites have shown incredibly interesting optoelectronic properties such as a direct and tunable bandgap. Furthermore, perovskites do not appear to suffer from some of the negative effects other types of light-sources suffer from. The widely known efficiency roll-off effect might not be as detrimental due to the nature of the perovskite material. Moreover, bright triplet emission has been observed in perovskites. Perovskites definitely are interesting light emitters and even more so when they are considered for high current density applications. Reports show PeLEDs reaching an EQE of over 14.36 %, at IMEC efficiencies around 4 % had already been achieved. On top of that the device stability is far from optimal. In IMEC, devices had a typical lifetime of several minutes although hour-long stable operation has been reported.[17] Both of these properties remain a problem to make real-world applications and further advancements are necessary.

The goal of the thesis was to optimize the method, the employed perovskites and the LED stack to attain a robust manufacturing method achieving high external quantum efficiencies around 10 % and hour-long lifetimes. To reach these results the focus was directed towards quasi 2 dimensional organic/inorganic lead halide perovskites. Most research in PSC was focused around methylammonium lead iodide hence this was chosen as building block to base further development on. To form 2 dimensional materials butylammonium was chosen. These materials result in infrared light emission but can serve as a guide to achieve similar results in the visible light range. Next to this, various characterization techniques had to be explored to get a good understanding of these new materials and their typical behaviour. Furthermore, insights in the device characteristics were necessary to base further improvements on.

1.5 Approach

As a first step the perovskite layer has to be optimized, careful tuning of the precursors results in different compositions. Each composition will be used in a standard device stack and assessed by measuring their lifetime and EQE. Simultaneously, characterization techniques such as x-ray diffraction, scanning electron microscopy and photoluminescence will be used to find out what

makes this material a better light emitter. Next, the device structure will be optimized by finding the most optimal transport layer. The cavity of the diode will then be optimized by tuning the thickness of the injection layer. Finally, interesting phenomena such as ion movement and their consequences are looked into. This method resulted in PeLEDs with an EQE above 10 % and a lifetime of several hours.

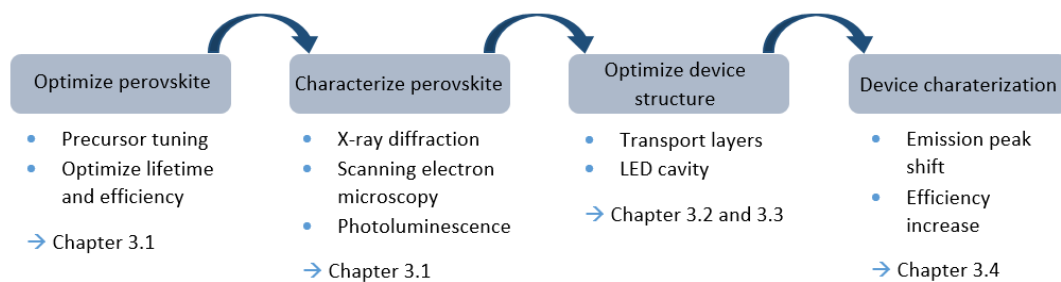


Figure 1.13: Schematic overview of the approach that was taken in this thesis.

Chapter 2

Fabrication Technique and Measurement Setup

This chapter gives details on the employed materials and how they should be used. The standard device stack is shown in Figure 2.1. In the manufacturing of the LED, two layers are deposited by spin coating, namely the hole transport layer (HTL) and the emissive layer. First, a detailed description is given of the required precursors for both layers. Afterwards, the fabrication of a typical PeLED is explained in a step-wise approach going through each layer from bottom to top. Finally, the self-build measurement setup, used for optical and electrical measurements, is introduced in detail. Other measurements techniques such as X-ray diffraction and photoluminescence are assumed to be well-known.

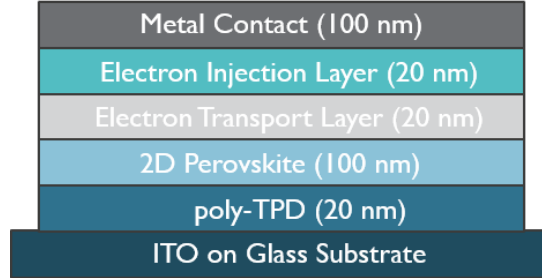


Figure 2.1: Schematic of the device stack build up of a standard PeLED. In this case the HTL and perovskite layer are spincoated. The other layers are thermally evaporated.

2.1 Precursor solution preparation

2.1.1 Poly-TPD

The organic molecule poly[N,N' -bis(4-butylphenyl)-N,N' -bis(phenyl)-benzidine] also called poly-TPD was used as HTL. To make the solution 6 mg of poly-TPD is weighed and dissolved into 1 ml chlorobenzene (CB). It is then put on a hotplate at 60°C while being stirred by a stirring magnet in N₂ atmosphere. When the poly-TPD is fully dissolved the solution is filtered with a 5 µm PTFE filter giving the final solution.

2.1.2 Perovskite

Most of the early steps taken in perovskite LEDs come directly due to materials and technology used in perovskite solar cells. However these materials have a low exciton binding energy resulting

Table 2.1: The percentages, molar concentration and concentration of BAI that is additionally added to the perovskite precursor to create 2D perovskites.

Additional % BAI	Molar Concentration (M)	Concentration (mg/ml)
0	0	0
10	0.03	6.032
20	0.06	12.064
30	0.09	18.096
40	0.12	24.128
50	0.15	30.16
60	0.18	36.192
70	0.21	42.224

Table 2.2: The amounts of MAI and MABR needed to form a stoichiometrically correct perovskite film. These values are used for 3 ml of solution.

(MAI:MABr)	m_{MAI} (mg)	m_{MABr} (mg)
(100:0)	30	0
(85:15)	25.5	3.2
(75:25)	22.5	5.3
(65:35)	19.5	7.4
(55:45)	16.5	9.5
(45:55)	13.5	11.65
(35:65)	10.5	13.8
(25:75)	7.5	15.9

in low EQE values. Stable excitons are one option so that charge carriers get the chance to recombine radiatively. The approach here to achieve this is to increase the exciton binding energy by incorporating large cations in the perovskite film forming a so called quasi two-dimensional perovskite. These large cations will separate the individual perovskite layers, thus creating a layered quantum well like structure.

The perovskite is spincoated in a two-step method, hence two precursors are required. The method builds on a base recipe that gives a normal three-dimensional perovskite film and can be tuned by including additives that result in ruddlesden popper phase perovskites. The first step is made by dissolving lead iodide (PbI_2) at a molar concentration of 0.3M or a concentration of 138,2 mg/ml in dimethylformamide (DMF). For each ml of DMF 21.66 μ l of dimethylsulfoxide (DMSO) is added. Confinement is induced by adding butylammonium iodide or BAI ($C_4H_{12}IN$) as percentages of the molar concentration of PbI_2 . To better dissolve the powders, the solution is placed on a hotplate while being stirred. Table 2.1 shows an overview of the required amount of BAI.

The second step contains methylammonium iodide (MAI) and methylammonium bromide (MABr) dissolved into isopropanol (IPA). For a stoichiometrically correct perovskite 10 mg/ml of MAI is required. The molar concentration is held constant when halides are mixed to achieve bandgap tuning. From this the amount of required MABr can be calculated. The exact values for a wide range of solutions are listed in Table 2.2.

2.2 Device fabrication

Substrates with a thickness of 1.1 mm were used that have 16 indium tin oxide (ITO) stripes, 8 on each side. Figure 2.2 a) shows a schematic of the substrate, the light grey area indicates the ITO stripes while the darker grey indicates the device area. The device area has a silicon nitride (Si_3N_4) pixelated pattern which serves as edge cover layer (ECL) to reduce the effects of sharp ITO edges leading to shorts and large leakage currents. Additionally, the patterning splits up the active area of the sample in small pixels. Figure 2.2 b) shows how the active area is pixelated and the pixel size.

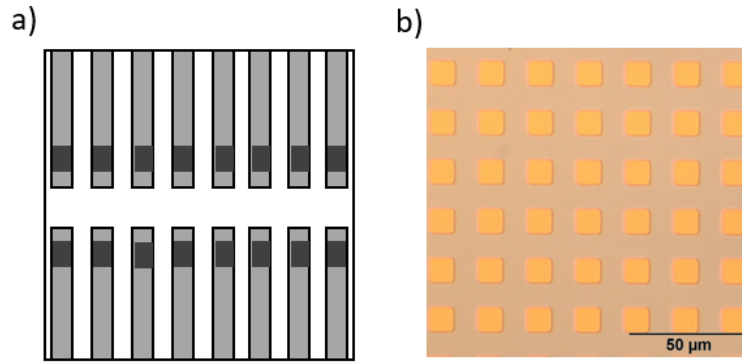


Figure 2.2: a) Schematic of the pixelated ECL substrate. The light grey area indicates ITO, the darker grey represents the pixelated area. b) Microscope image of a pixelated substrate used for PeLEDs.

The substrates were cleaned by sonication which starts by manually washing in Extran soap and deionized water (DIW) after which they are sonicated for at least 5 minutes. The solution is then diluted by continuously adding DIW to it until no trace of the soap can be seen. The samples are then properly rinsed with DIW and transferred into a different beaker containing only DIW after which they are sonicated again for at least 5 minutes. Afterwards the substrates are placed into a beaker of acetone and sonicated for at least 5 minutes. Finally the substrates are placed into a beaker of isopropanol and are again sonicated for 5 minutes. The substrates are then dried with a N_2 gun and stored inside a glovebox if processing isn't immediately performed.

Before processing starts the substrates are exposed to an oxygen plasma for at least 5 min at 200 W. First the HTL is statically spincoated at 1000 rpm for 30 seconds with an acceleration of 5000 rpm/s. The layer is then dried on a hot plate at 150°C for 20 minutes. Afterwards it is subjected to an oxygen plasma at 100W for 1 second to improve the wetting. A perovskite layer is then spincoated in a 2 step method. First, the PbI_2 and BAI solution is statically spincoated for 30 seconds at 3000 rpm with an acceleration of 2000 rpm/s. After which $50\text{ }\mu\text{l}$ of MAI:MABr solution is dropped on top of the spinning sample. Simultaneously, the spincoater will slow down to 2000 rpm whilst the acceleration and duration is the same as in the first step. When completely finished the layer is dried on a hotplate at 80°C for 30 minutes.

It has to be noted that several precautions have to be taken to ensure high quality perovskite films in every experiment. Perovskites are known to be very sensitive materials and lab to lab variation is often observed. Before all spincoating experiments, the spincoater is prepared by covering all its sides with aluminium foil and making sure that no oxygen is present in the glovebox. During the spincoating a minimal amount of movement and gas flushing should be used in the glovebox as they can cause dust particles to hit the film resulting in artefacts. Afterwards the spincoater is cleaned completely and all trash is taken out of the glovebox to prevent it from making additional dust particles. Still, with all these things under consideration, sample to sample variation can be

observed.

An evaporation chamber from the Kurt J. Lesker company is used to deposited the ETL, EIL and metal contact. On the edges of the samples the spincoated layers are scratched away so that a metal contact can be evaporated on to the ITO stripes. The evaporation chamber can fit 9 samples at once, which can be patterned with shadow masks. Once in the chamber a rectangular shadow mask shown in Figure 2.3 b) is placed on the samples which covers the edges all around. This is to make sure that the ETL cannot form a blocking layer between the ITO strip and the metal contact. After the deposition of the ETL the shadow mask is switched to the mask shown in Figure 2.3 c). The mask creates a long metal strip over all the devices and results in 12 LEDs and 4 metal contacts, 6 LEDs on each side sandwiched between 2 contacts.

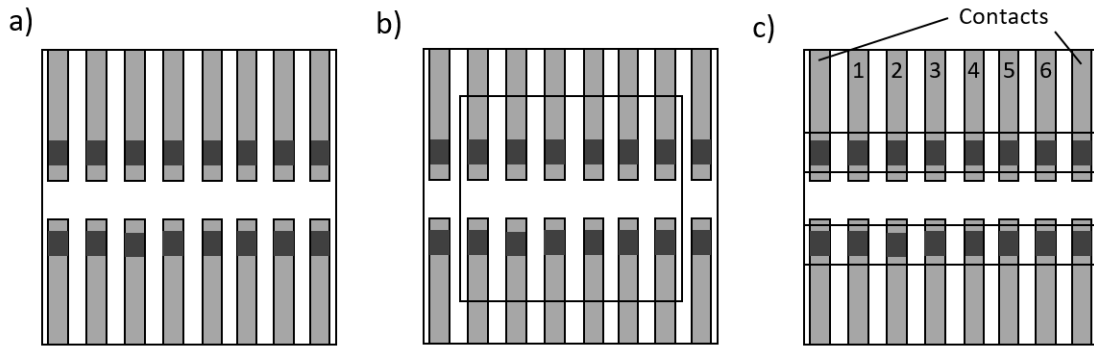


Figure 2.3: a) A schematic on an unprocessed sample showing ITO stripes. The slightly darker squares indicated the pixelated active area. b) A schematic of which area the rectangular mask covers when the ETL is deposited. c) A schematic of the shadow masks that is used to deposit the EIL and the metal contacts.

2.3 Measurement setup

Due to the often short lifetime of the manufactured devices a measurement setup was needed that could extract all the valuable data from the devices before severe degradation occurred. To collect as much light as possible in a short timeframe an integrating sphere was used as foundation. A sampleholder was fitted on top, while a photodiode and a fiberglass cable leading to a spectrometer were attached to the side. A schematic of the setup can be found in Figure 2.4. The collected data allows to calculate the external quantum efficiency. The biasing and IV characteristics measurements are performed by an Agilent 4155C Semiconductor Parameter Analyzer, the photocurrent ($I_p h$) is measured by a Newport 818-SL-L Silicon photodetector and the spectral data is acquired with a Flame Spectrometer by Ocean Optics.

The measurement is operated by using a self written LabVIEW program. A standard measurement sweeps through the following steps, first a voltage sweep is performed to acquire the IV data of the LED while simultaneously measuring the photocurrent with the photodiode. Afterwards a constant current is applied to measure the lifetime characteristics. After each preset interval the photocurrent and spectrum are measured. The acquired data is saved in a text file, after which it can be used to calculate the EQE of the individual LEDs. To simplify this entire process a Python script was written which takes the raw data files and outputs a processed data file containing the EQE, emission peak position and radiance of the devices.

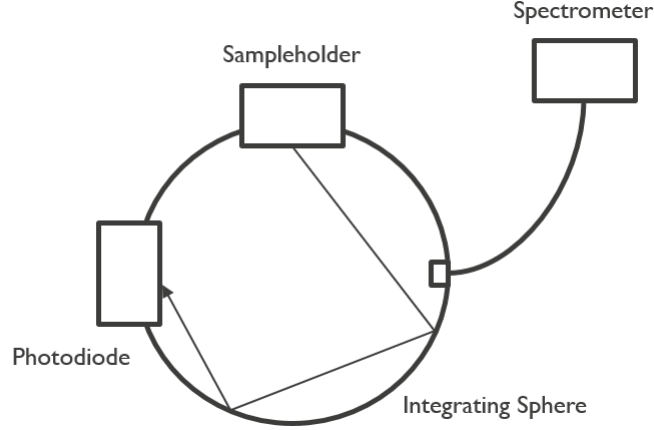


Figure 2.4: Schematic of the constructed measurement setup around an integrating sphere.

2.3.1 Calculating external quantum efficiency

An important quantity that is commonly used to evaluate a light source is the external quantum efficiency. This value is the ratio of the amount of photons that are emitted by the source over the amount of electrons that were used to power the light source and is always given as a percentage, Equation 2.1 shows the formula. The constructed measurement setup can measure all the required data to calculate this value. However several steps are required to get to the amount of electrons and photons. To keep a good overview the calculation is split up in 2 separate parts.

$$EQE = \frac{\text{Emitted Photons}}{\text{Injected Electrons}} \quad (2.1)$$

Amount of emitted photons

To calculate the amount of photons that are emitted from a lightsource several approaches can be taken. One way is to look at the photocurrent (I_{photo}) measured by the photodiode which is related to the emitted power at each wavelength ($P(\lambda)$) multiplied the responsivity of the photodiode at each wavelength ($R(\lambda)$). By integrating this product over the entire spectrum the photocurrent is found.

$$I_{photo} = \int P(\lambda)R(\lambda)d\lambda \quad (2.2)$$

This formula contains $P(\lambda)$ which is directly related to the amount of photons emitted at each wavelength per second ($n(\lambda)$) and the energy one such photon has, which is equal to Planck's constant (h) times the frequency (f) of the photon. $P(\lambda)$ can thus be written as:

$$P(\lambda) = n(\lambda)hf \quad (2.3)$$

By using the dispersion relation which states $c = \lambda f$ where c is the speed of light and rewriting the equation for $n(\lambda)$ the previous equation becomes.

$$P(\lambda) = \frac{n(\lambda)hc}{\lambda} \quad (2.4)$$

Unfortunately, in the build measurement setup $P(\lambda)$ can not be measured directly. However the same result can be achieved by using the emission spectrum in a clever way, as this can be rewritten to the normalized power spectrum ($P^N(\lambda)$). This can be found by dividing the power at each wavelength by the total emitted power (P_{em}), for which is known that:

$$P_{em} = \int P(\lambda) d\lambda \quad (2.5)$$

Thus the normalized power spectrum is equal to:

$$P^N(\lambda) = \frac{P(\lambda)}{P_{em}} = \frac{P(\lambda)}{\int P(\lambda) d\lambda} \quad (2.6)$$

By now invoking equation 2.4 this can be rewritten to the following:

$$P^N(\lambda) = \frac{n(\lambda)hc}{\lambda \int \frac{n(\lambda)hc}{\lambda} d\lambda} = \frac{n(\lambda)}{\lambda \int n(\lambda)/\lambda d\lambda} \quad (2.7)$$

The amount of photons at each wavelength $n(\lambda)$ is still an unknown quantity, however it can be substituted by the emission spectrum $n_{sp}(\lambda)$. $n(\lambda)$ has a certain distribution that it shares with $n_{sp}(\lambda)$. Normalizing both makes them identical and since Equation 2.7 has $n(\lambda)$ on both sides of the fraction the emission spectrum can be used instead of the actual amount of photons at each wavelength.

$$n^N(\lambda) = \frac{n(\lambda)}{N_{total}} = \frac{n_{sp}(\lambda)}{N_{sp}} = \frac{n(\lambda)}{\int n(\lambda) d\lambda} \quad (2.8)$$

$$\frac{n(\lambda)}{\lambda \int n(\lambda)/\lambda d\lambda} = \frac{N_{total}n(\lambda)}{\lambda N_{total} \int n(\lambda)/\lambda d\lambda} = \frac{n^N(\lambda)}{\lambda \int n^N(\lambda)/\lambda d\lambda} \quad (2.9)$$

$$\frac{n^N(\lambda)}{\lambda \int n^N(\lambda)/\lambda d\lambda} = \frac{N_{sp}n^N(\lambda)}{\lambda N_{sp} \int n^N(\lambda)/\lambda d\lambda} = \frac{n_{sp}(\lambda)}{\lambda \int n_{sp}(\lambda)/\lambda d\lambda} \quad (2.10)$$

Thus the normalized power spectrum $P^N(\lambda)$ can be written as.

$$P^N(\lambda) = \frac{n_{sp}(\lambda)}{\lambda \int n_{sp}(\lambda)/\lambda d\lambda} \quad (2.11)$$

The photocurrent can thus eventually be rewritten as the following:

$$I_{photo} = P_{em} \int P^N(\lambda) R(\lambda) d\lambda = P_{em} \int \frac{n_{sp}(\lambda) R(\lambda)}{\lambda \int n_{sp}(\lambda)/\lambda d\lambda} d\lambda \quad (2.12)$$

The total amount of emitted photons N can also be found by rewriting equation 2.4 and integrating over all wavelengths.

$$N = \frac{1}{hc} \int \lambda P(\lambda) d\lambda \quad (2.13)$$

By using equation 2.6 this can be rewritten too:

$$N = \frac{P_{em}}{hc} \int \lambda P^N(\lambda) d\lambda \quad (2.14)$$

Now equation 2.12 can be used to get rid of the unknown P_{em} . This gives the total amount of photons that were emitted so that all terms in the equation are known.

$$N = \frac{I_{photo} \int \lambda P^N(\lambda) d\lambda}{hc \int P^N(\lambda) R(\lambda) d\lambda} \quad (2.15)$$

Finally equation 2.11 can be filled in giving the amount of emitted photons only in measured quantities.

$$N = \frac{I_{photo} \int \frac{\lambda n_{sp}(\lambda)}{\lambda \int n_{sp}(\lambda)/\lambda d\lambda} d\lambda}{hc \int \frac{n_{sp}(\lambda) R(\lambda)}{\lambda \int n_{sp}(\lambda)/\lambda d\lambda} d\lambda} \quad (2.16)$$

Amount of injected electrons

The amount of supplied electrons to the LED can be found easily by dividing the current I_{device} delivered to the device by the elementary charge constant q .

$$Amount\ of\ electrons = \frac{I_{device}}{q} \quad (2.17)$$

2.3.2 Calibration

To calibrate the measurement setup an OLED from the OLED research group at IMEC was used. This device was measured in their dedicated and calibrated setup and then measured in this setup. A correction factor was subsequently introduced in the python script doing the EQE calculations to match the actual value with the measured values. A more proper calibration could have been done with a calibrated quartz tungsten halogen (QTH) lamp designed for this purpose. Although the calibration might not be ideal, the measured values should give a good indication of the actual device characteristics and allow devices to be compared to each other.

Chapter 3

Results and Discussion

In this chapter the attained results are presented together with insight in their possible consequences and origin. First, the perovskite layer is optimized to increase the efficiency and lifetime of the PeLEDs. To this end the layers are tested by using them in the default device structure. Afterwards, the layers are characterized by X-ray diffraction, scanning electron microscopy and photoluminescence. In the second part of this chapter, a better electron transport layer is sought by altering the default device stack and looking at the device characteristics. On top of that, the emission zone of the optimized device structure is sought to optimally tune the LED cavity. Finally, two interesting phenomenon possible related to ionic movement in the perovskite are looked into.

3.1 Perovskite layer optimization

The first step in order to achieve the goal of highly efficient and stable perovskite LEDs was finding the most optimal amount of confinement. By careful tuning of the amount of BAI present in the perovskite precursors Ruddlesden-Popper phase perovskites with various orders can be realized. In practice BAI was added in steps equal to 10 % of the normal molar concentration of PbI_2 needed to make a regular 3D perovskite film. These layers were then used in default device structure shown in Figure 2.1 where the electron transport and injection layer were made with the Novaled materials mentioned in Section 3.2.

Table 3.1: Overview of results showing the influence of the amount of BAI in the perovskite film. Since only very few 10% BAI devices were measured no average value was calculated.

Additional BAI (%)	average EQE (%)	max EQE (%)	Lifetime
3D	0.321 ± 0.001	0.322 ± 0.002	> 10 minutes
10	/	4.849 ± 0.009	> 10 minutes
20	4.830 ± 0.004	5.656 ± 0.008	> 1 Hour
30	3.788 ± 0.003	4.119 ± 0.006	> 10 minutes
40	3.912 ± 0.003	4.162 ± 0.006	> 10 minutes
50	6.58 ± 0.01	10.48 ± 0.02	T90 of 3.5 Hours
60	1.369 ± 0.004	1.825 ± 0.009	> 10 minutes

A comparison between typical devices of each percentage is shown in Figure 3.1. The EQE increases gradually to a more stabilized emission, although some show an initial decrease. This effect was persistent over several device runs and is occasionally even more severe than shown here. The best devices were those that had 50 % additional BAI which in this initial test almost attained an EQE of 7 %. An overview of the influence the BAI has on the perovskite film can

be found in Table 3.1. A recurring behaviour in these devices is that their emission wavelength changes and saturates around 750 nm. There is a slight difference of a few nanometer between the 10 % device and the others, however it is hard to draw a conclusion from this due to the resolution of the spectrometer. A notable difference exists in the wavelength of the emission onset, higher BAI percentages seem to redshift the emission slightly. This could be explained by the fact that BAI also contains one iodide ion which can now also participate in the crystal formation. As a result the initial ratio between iodide and bromide coming from MAI and MABr is now tilted slightly more towards iodide. To further explore why 50 % BAI gave the best result several characterization methods were used.

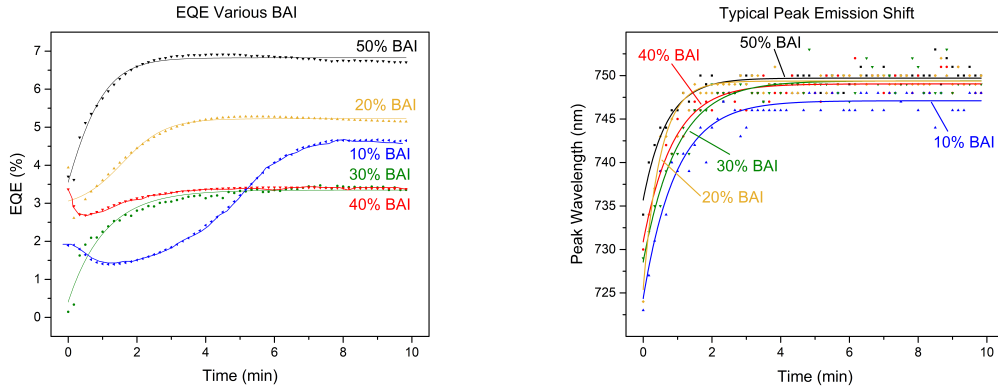


Figure 3.1: left) A comparison between the EQE values through time of PeLEDs made with different BAI percentages in their precursors. A guide to the eye has been plotted to show the trend in the datapoints. right) The typical emission peak shift observed in PeLEDs having different BAI concentrations. Nevertheless, these curves all stabilize around the same wavelength. A guide to the eye has been plotted to better show the characteristics of the data points.

Photoluminescence

Photoluminescence measurements were performed to gain insight in the photo physics, relaxation processes and relaxation lifetime. Perovskite films were spincoated on poly-TPD covered 3 by 3 cm glass substrates to exclude any surface influence on the film morphology. Figure 3.2 left) shows a comparison of the normalized PL spectra of each film. At intermediate percentages of BAI several emission peaks appear indicating the existence of multiple phases.

Figure 3.2 right) shows measurements performed on a 50 % BAI sample but at different spots. From spot to spot a substantial difference exists in the PL spectra, mainly in the relative intensity of the peaks. Overall these measurements illustrate the main issue of the 2 step spincoating process. A large inhomogeneity exists between the center and edge of the film. Similar measurements on a 3D perovskite film were performed and can be found in Figure 3.3. Here, non-uniformity was not present as the 3D samples appear to have the same phase everywhere which hints towards the large cations having an influence on the film formation in the 2D material. Both 3D spectra show only a change in PL intensity when comparing different spots of the sample which might be related to a thickness variation due to the spincoating. An interesting thing to note is the amplified spontaneous emission (ASE) in Figure 3.3 left). This is an indication that lasing could possibly be achieved with perovskite layers.

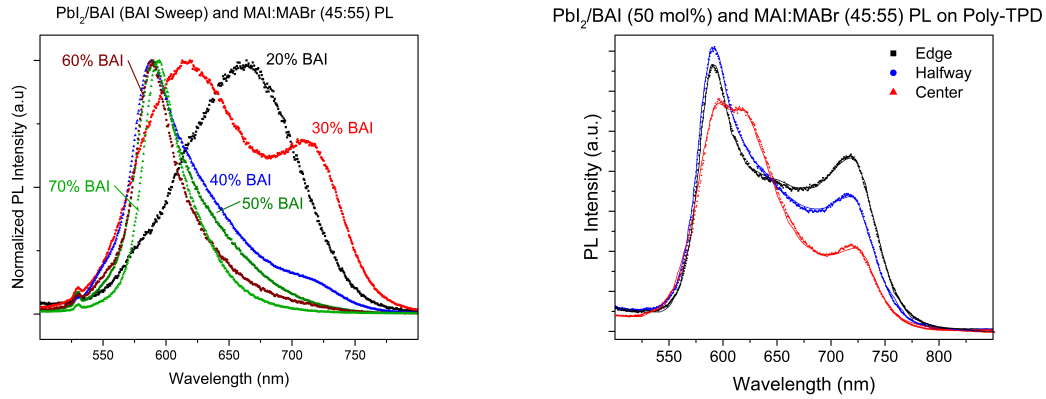


Figure 3.2: left) Normalized PL spectra of 2D perovskite films differing in their BAI percentage. All these measurements were taken in the center of the sample. The 50% BAI spectrum differs from the one shown in the other results again indicating that there is quite some variation between separate perovskite layers. right) PL measurement on the same perovskite film as in the left graph, spincoated on a Poly-TPD surface to mimic the film found in actual devices.

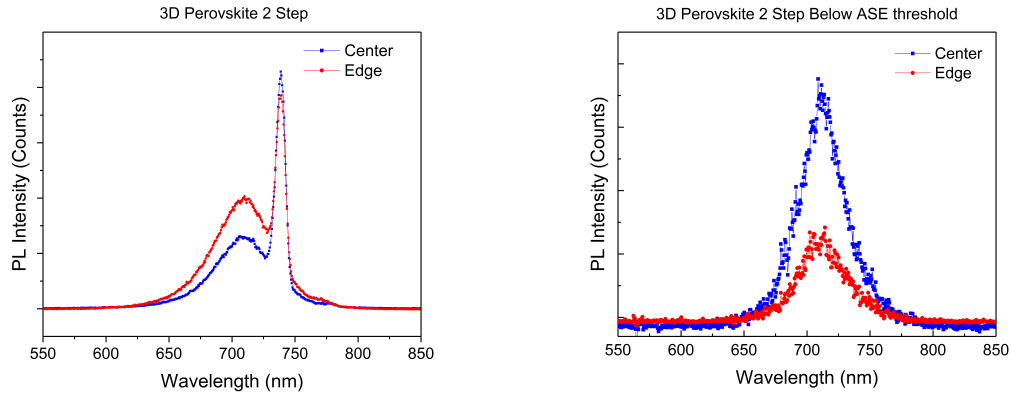


Figure 3.3: left) PL measurement on 3D perovskite film with a MAI:MABr ratio of 45:55. No large difference can be found between the edge and the center of the film indicating a more uniform film. right) PL measurement on the same sample as on the left with the laser intensity decreased so its power is insufficient to induce ASE.

Time resolved photoluminescence

The decay characteristics of the charge carriers were measured by time resolved PL. To do this the PL spectrum is measured at various intervals after an excitation pulse of the laser triggers the tool. Afterwards these spectra can be integrated and the decay characteristics can be fitted. Figure 3.5 shows a comparison of the decay characteristics of the integrated intensities for a 3D perovskite film and a 2D 50% BAI film. The individual spectra at delay times around the decay lifetimes can be found in Figure 3.4. In the 3D perovskite spectrum there is only one peak centered around 710 nm. The 2D spectrum on the other hand has 3 distinct peaks, a very broad and low intensity peak around 510 nm and 2 much sharper peaks at around 585 nm and 725 nm. The broad peak likely comes from the poly-TPD layer while the 2 other come from the perovskite. The poly-TPD peak seems to have a sufficiently long lifetime so that it could be assumed to be a part of the background present in all the measurements. The peak at 725 nm might have a similar origin as the one at 710 nm as they possibly both represent 3D parts of the material, the slight difference

in wavelength could be caused by the additional iodide present in the 2D film due to the BAI molecules.

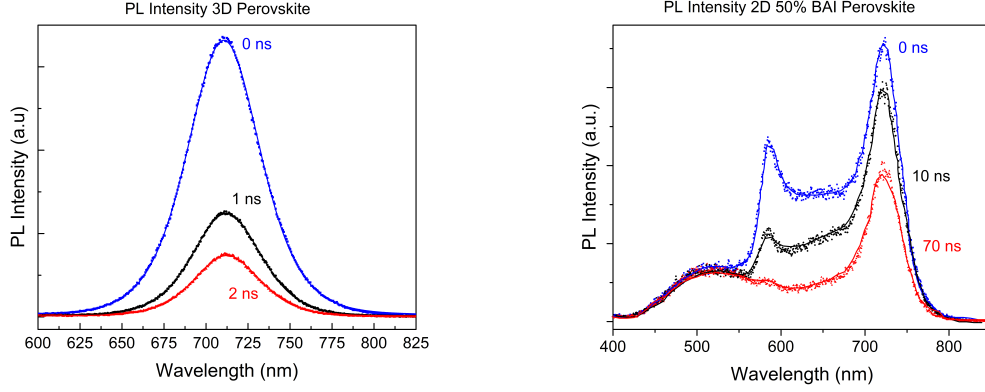


Figure 3.4: PL spectra taken during time resolved PL measurements, from these spectra the decay lifetimes can be found. left) Here 3 spectra of a 3D samples are show with each having one ns delay between them. right) Here the spectra were chosen to be almost equal to the observed decay lifetimes of the 2D samples, hence why the spectra at 10 ns and 70 ns of delay are shown.

The fitting of the integrated data was done with the fitting tool in Origin. As can be seen in the detailed spectra in Figure 3.4, the 3D perovskite only has one PL peak so a single exponential decay gave a good fit. To properly fit the 2D perovskite peaks a double exponential decay was used. The decay constant τ for the 3D perovskite was equal to 1.28 ns while the decay constants τ_1 and τ_2 for the 2D perovskite were equal to 10.14 ns and 68.93 ns respectively, with the longest lifetime of the two coming from the peak at 725 nm. This increase in decay lifetime indicates that the additional BAI molecules increase the exciton lifetime possibly by decreasing the amount of trap assisted recombinations. The peak around 585 nm indicates that there might be a second phase present in the perovskite film that does not emit light under normal operation.

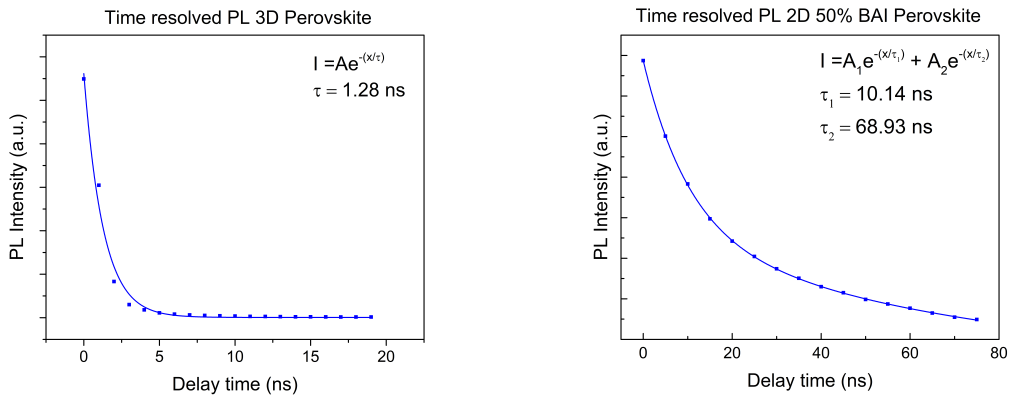


Figure 3.5: The time resolved data of both a 3D and 2D film having 50% BAI acquired by integrating several PL spectra taken at various delay times. The data was fitted with the fitting tool in Origin and the resulting curves have been plotted on top of the datapoints. The 3D film has a decay lifetime of 1.28 ns whereas the 2D film, which was fitted with a double exponential decay, has lifetimes of 10.14 ns and 68.93 ns.

X-Ray Diffraction

To learn more of the crystallinity and the perovskite phases inside the film x-ray diffraction (XRD) measurements were performed. Perovskites were spincoated on ITO/glass substrates covered with poly-TPD to ensure that identical films were used as found in devices. A poly-TPD film was measured first so that it could be subtracted as background later.

Figure 3.6 shows a comparison between a 3 dimensional perovskite and 2 dimensional perovskite having 50% additional BAI, both films were made with a 45:55 MAI:MABr ratio. The 3D film shows the standard perovskite peaks at angles of 14.2° and 26.6° and a very small peak at 32.2° whom respectively belong to the (110), (220) and (222) directions. Looking at the 2D perovskite the scan is less clear. The perovskite peaks at 14.2° and 26.6° barely overcome the noise of the measurement. The crystallinity of the 2D perovskite is thus substantially worse then the one of the 3D perovskite. The weak signal might be caused by very small and spread out 3D perovskite crystallites in the 2D film. Additionally, no 2D phase can be observed although plenty of large cations are present in the film. It is possible that instead of a layered structure the film looks more like a micellar structure where small 3D perovskite crystallites are completely surrounded by the large cations.

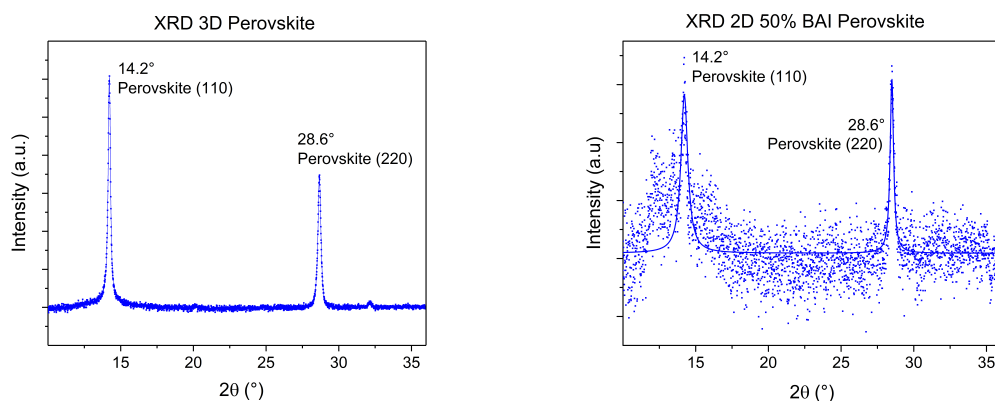


Figure 3.6: left) XRD spectrum of a 3D perovskite film showing typical perovskite peaks at 14.2° and 26.6° as well as a very small peak at 32.2° . right) The XRD spectrum of a 2D perovskite having 50% additional BAI. Here the typical perovskite peaks are much less pronounced indicating a smaller degree of crystallinity. A guide to the eye has been plotted on the datapoints to better illustrate the behaviour.

Scanning Electron Microscopy

Details on the surface coverage, layer cross section and roughness of the film were uncovered by doing scanning electron measurements. The measurements were performed on perovskite films deposited on glass substrates covered with poly-TPD to ensure that the measured film is identical to the one in actual PeLEDs. Figure 3.8 compares two SEM images of a 2D 50% BAI and 3D perovskite of which the measurement is taken where a device is normally situated. Figure 3.7 shows a schematic of where the normal SEM and cross sectional SEM measurements were taken. The 3D film completely covers the substrate while some small crystallites appear to lie on top of the film. On the other hand, the 2D film seems very flat but does not completely cover the film since several pinhole-like structures can be seen.

Next to the normal SEM measurements cross section SEM measurements were made on the same samples by cleaving and viewing them from an angle, Figure 3.9 shows both types of samples.

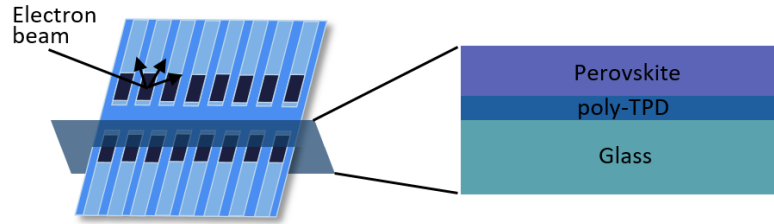


Figure 3.7: Schematic of the SEM and cross sectional SEM measurements to indicate which exact spot of the sample was measured.

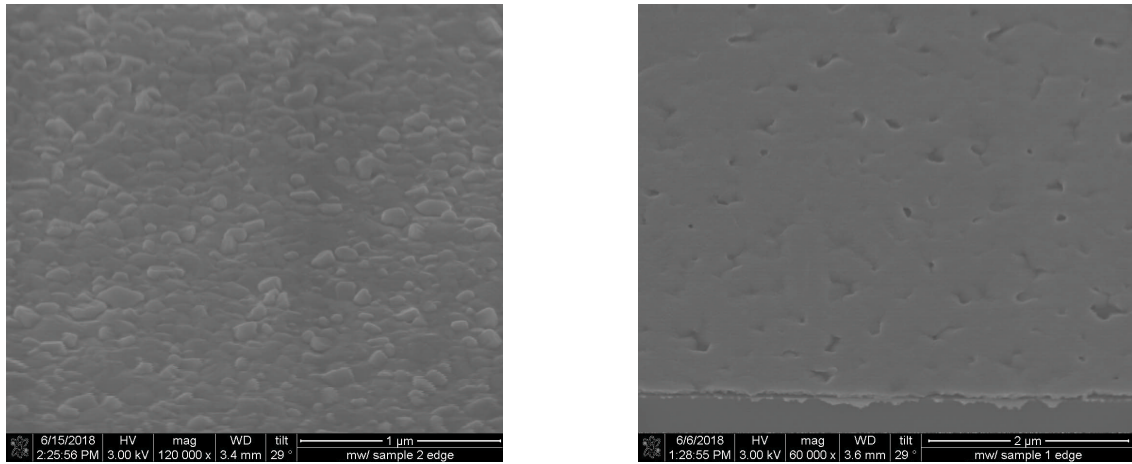


Figure 3.8: left) An SEM image of a 3D perovskite film on a poly-TPD surface. right) An SEM image of a 2D 50% BAI perovskite film on a poly-TPD surface.

In the case of the 3D film, the thickness variation due to the grains is in the order of 30 nm or even higher which aligns well with the roughness observed with SEM. For the 2D film the situation is completely different, this film is much smoother without actual grains. The estimated thickness also appears to be lower than expected, however thinner perovskite layers are beneficial for EL.

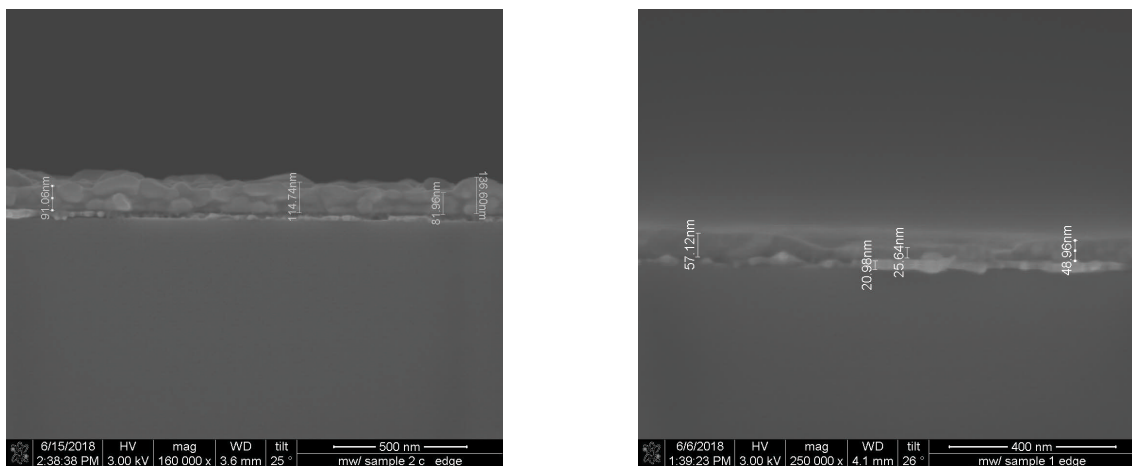


Figure 3.9: Crosssectional SEM images of 3D and 2D perovskite films respectively made on a Poly-TPD surface. Thickness estimations are made in the image.

Additional measurements were performed on various perovskite samples having different BAI percentages and anneal temperatures. These measurements can be found in Appendix A. 30 and 70% samples are shown to give insight in the effect of the BAI concentration. Overall, they look quite similar to 50% BAI since they all appear to have some pinholes. The 30% sample seems to have larger crystallites than a 3D sample while the 70% sample has larger crystallites that look more like flakes than small grains. The temperature was found to have an influence on the crystallite size in the film, lower T results in slower crystallization and thus lead to smaller and more crystallites. The exact opposite is the case when higher T are used, here the crystallites are larger and again look more like flakes than grains.

Optical Microscopy

Optical microscopy was performed on 2D 50% BAI perovskite films and revealed several stripes on the film, Figure 3.10 shows microscope snapshots in bright and dark field mode. The stripes have an outward direction coming from the middle of the sample and seem to be the results of spincoating. The stripes seem to be build out of small dots resembling pinholes at the surface. Out of fear that these pinholes completely penetrate the perovskite layer, chlorobenzene was dropped on top of a sample. In the scenario that they actually penetrate the entire layer the chlorobenzene could reach the HTL beneath and dissolve it. However, no effect on the HTL was observed which suggests that these structures are only present at the surface.

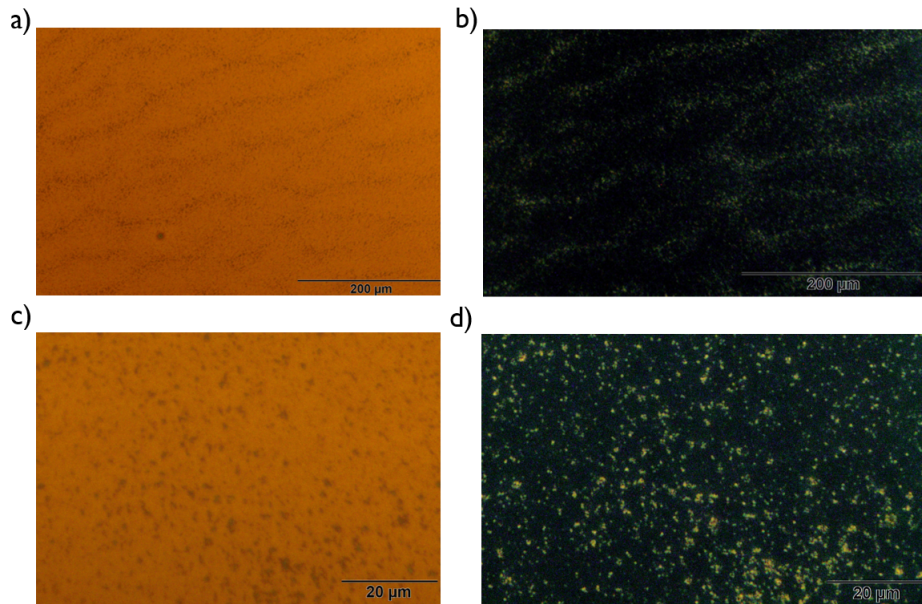


Figure 3.10: a) and b) show a bright and dark field image of a 50% BAI 2D sample respectively. c) and d) show a bright and dark field image under stronger magnification of a 50% 2D sample respectively.

What exact implications these pinholes have on the device performance is unknown. Optically this extra roughness could lead to better outcoupling of the generated light. Electrically the pinhole-like structures could lead to much higher local current densities due to a lower resistance in the thinner perovskite. Nevertheless, they do not appear to have a negative effect on the device performance since this film performs better than all the other alternatives that were tested.

Anneal temperature

In literature it is common that perovskite layers designed for light emission are annealed at relatively low temperatures and for short periods of time. These lower temperatures are said to result in smaller crystallites giving more confinement. In all the previous experiments the perovskite layers were always annealed at 80°C for half an hour. To test if lower temperatures and short anneal times would be beneficial devices were made with layers annealed at 60°C and 70°C as well as devices annealed for shorter times in increments of 5 minutes. Figure 3.11 shows the comparison of the typical EQE characteristics at lower anneal temperatures. No increase in the EQE nor the stability was observed, the initially used 80°C results in the best performance. The data for different anneal times can be seen in Table 3.2. It is difficult to say if there is any major influence of the anneal time at all. The lower efficiencies measured for the 10 minute samples are quite likely some form of sample to sample variation due to the spincoating since the other times almost result in identical efficiencies.

Table 3.2: The average and maximum EQE values attained with various anneal times.

Anneal Time (min)	average EQE (%)	max EQE (%)
5	5.94 ± 0.01	7.58 ± 0.01
10	4.805 ± 0.004	5.287 ± 0.008
15	6.27 ± 0.01	6.59 ± 0.01
20	6.32 ± 0.01	7.13 ± 0.01
25	6.44 ± 0.01	6.55 ± 0.01

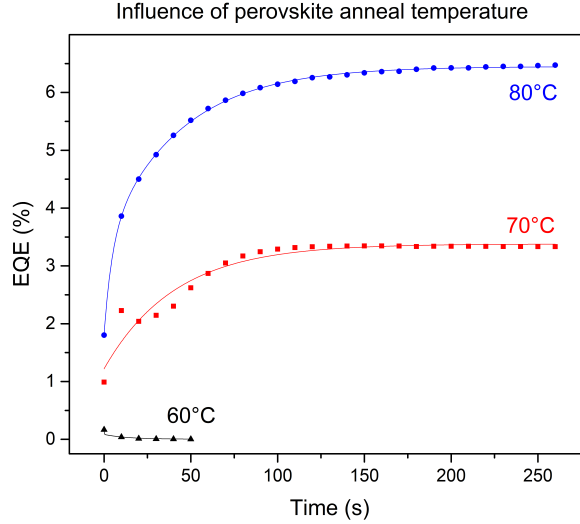


Figure 3.11: The average and maximum EQE measured in PeLEDs in which the perovskite layer was annealed for different amounts of time.

Optimized Perovskite LEDs

The most optimal perovskite was found to be when BAI was added equal to 50 % of the regular molar concentration for a 3D perovskite. Figure 3.12 left) shows several devices having 50% additional BAI in a stack containing the Novaled materials. Their EQE values after stabilization are

spread out over an interval of about 3% even though these devices all come from the same batch. This indicates that the sample to sample and device to device variation is quite large. However this comes as no surprise since the perovskite layer does show a degree of non-uniformity. The photoluminescence (PL) studies show this effect more clearly. On the right, the attained EQE values of the devices of several runs have been placed in a histogram to better show the recurrence of each efficiency. The accompanying Gaussian distribution has been plotted on top, the mean of the data is 6.58 with a standard deviation of 0.91. During the last device run some devices were even better, reaching EQE percentages of over 10 %, these were treated as an outlier and not included here. The characteristics of one of these devices can be found in Figure 3.14 right). The high efficiencies were likely the result from small improvements such as fresh materials in the evaporation chamber, a lower than usual vacuum in the chamber resulting in a better layer and a possible deviation during the spincoating of the perovskite.

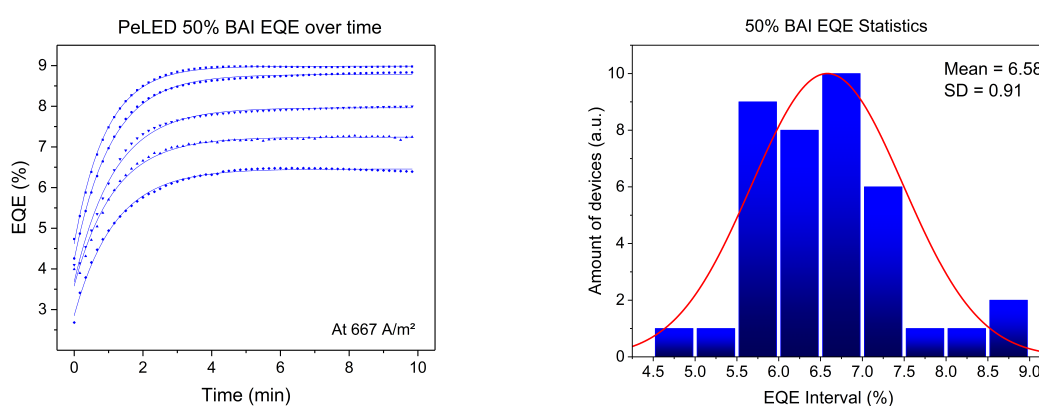


Figure 3.12: left) A comparison between several devices having 50% additional BAI. Due to device to device variation the spread between the data is about 3% in EQE. A guide to the eye has been plotted to show the trend of each set of data points. The error bars were not plotted since they are not larger than the symbols indicating the data points. right) A histogram of all 50% BAI PeLEDs which again shows their non-uniformity. The mean of the EQE is 6.58 % and the standard deviation is 0.91. Some outliers from the last device run have not been included into the histogram.

The stability characteristics of these devices were tested by measuring the devices at several current densities. At the moment, the lifetime of perovskite LEDs is often not reported which means there is a lack of convention to how these values should be accurately compared. The method chosen here resembles the one for OLEDs. In practice the devices are biased at a preset constant current and for the duration of the measurement the EQE and emission wavelength are tracked. Since the devices require a burn in, the start of the lifetime is taken after the maximum in efficiency is achieved. Here, the T_{90} i.e. the time after which the efficiency has dropped by 10% from its maximum value is reported. In the case of a device biased constantly at 667 A/m^2 this is equal to 3.5 hours. At a higher current density equal to 2000 A/m^2 a 50% device has a T_{90} of 17 minutes.

To observe if any form of roll off occurs in these devices the EQE was measured at several current densities. To do this a device would be biased for several minutes to allow it to reach stabilized emission, after this the applied current would gradually be ramped up in steps, at every step the device was again given up to half a minute to stabilize after which the EQE was measured. No longer times were used to avoid that degradation could occur skewing the data. Figure 3.14 shows EQE over the range of a few thousand A/m^2 . The initial part of the graph indicates that there is a roll on present in these devices, this could be related to traps existing in the perovskite layer. At lower current density not all these traps can be filled up and they thus diminish the

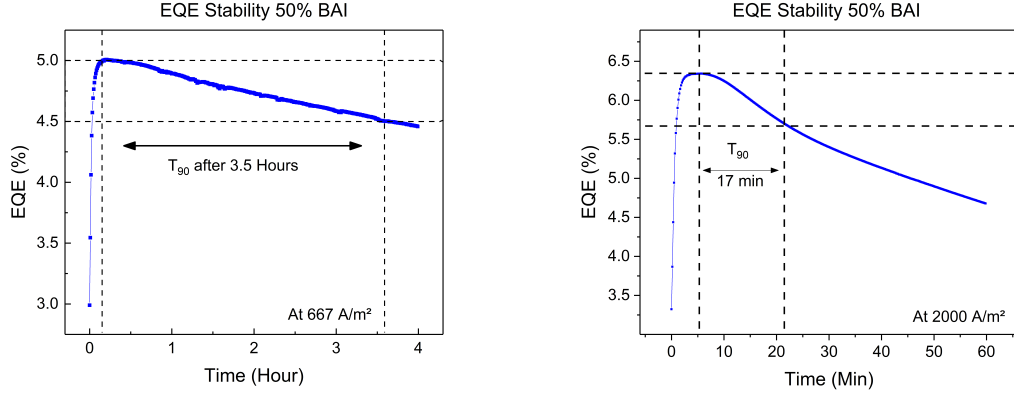


Figure 3.13: left) The lifetime of a 50% BAI PeLED biased at a constant 667 A/m^2 . The time after which ten percent of the maximum efficiency was lost is 3.5 hours. right) A 50% BAI device biased at a constant current density equal to 2000 A/m^2 , the T_{90} of the device is 17 minutes. In both graphs a guide to the eye has been plotted, the error bars have been left out since they were not larger than the symbols of the data points.

overall efficiency of the device. At slightly higher current densities these traps could all be filled so that they can be ignored and the device operates at its maximum attainable efficiency. For very high current densities a roll off can be seen were the device steadily drops in EQE as the current density increases. The effects causing this roll off are likely some bimolecular annihilations that lead to exciton quenching.

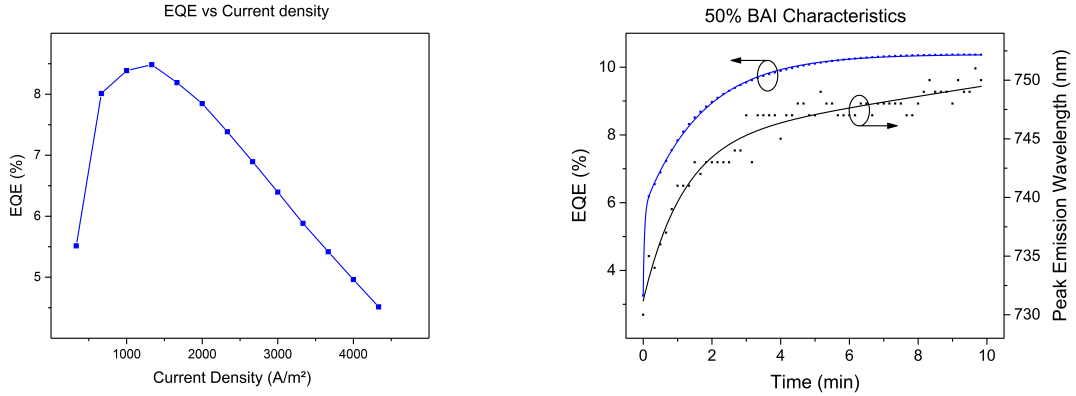


Figure 3.14: left) The EQE vs current density behaviour of a typical PeLED. At low current densities an efficiency roll on can be seen likely related to trap filling, at high current densities there is a roll off which might be caused by bimolecular annihilation. right) Device characteristics of the device that reached the highest overall efficiency, the EQE value after 10 minutes is equal to 10.48 ± 0.02 . Just like before the emission wavelength shifts from around 730 nm to 750 nm.

3.2 ETL alternatives

Simultaneous with the search for the most optimal perovskite layer, several electron transport layers were tested to improve the efficiency and lifetime. The most commonly used electron transport layer (ETL) in the perovskite LED research field is TPBi combined with LiF as injection

layer and aluminium as metal contact. However these materials did not result in very high efficiencies and a replacement was sought. Among the tested alternatives were Novaled transport material NET18 and its dopant NDN26, bathophenanthroline or Bphen which known for having a high mobility and 2,4,6-tris[3-(diphenylphosphinyl)phenyl]-1,3,5-triazine also known as PO-T2T. Figure 3.15 shows the chemical structure of the used electron transport layers, while Figure 3.16 shows the band alignment of the various ETL materials with the rest of the stack. Since the exact energy levels are not known for the 2D perovskite layer the energy levels from its 3D counterpart were used. In general due to the confinement in the 2D structures the energy levels should be higher than the ones shown here.

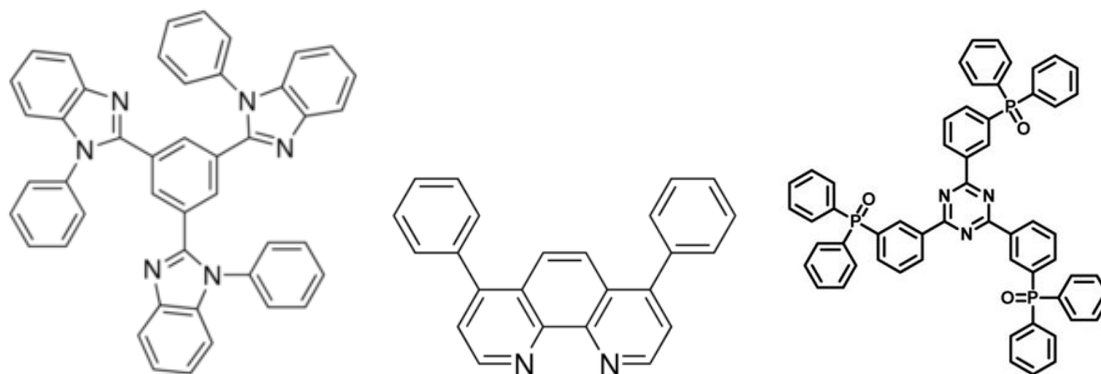


Figure 3.15: Chemical structures of the employed electron transport layers, from left to right the structures belong to TPBi, Bphen and PO-T2T.

Every material, with the exception of the Novaled materials, was tested by using 40 nm of it in a device stack. The rest of the stack consisted of 2 nm of 8-Quinolinolato lithium or Liq as injection layer and 100 nm silver as metal contact. The Novaled materials were used differently since this ETL has a specifically designed dopant to accompany it. Here, Novaled electron transport material NET18 is used together with its dopant NDN26. Unfortunately, no detailed information about the composition of these materials is made public. In a standard device, a 20 nm NET18 layer is evaporated as ETL followed by another 20 nm NET18 layer 5% doped with NDN26 to serve as injection layer. Again, to finish the stack 100 nm of silver is used.

Figure 3.17 shows a comparison between typical results achieved with each electron transport layer. Trendlines were fitted on the data points to give an indication of the overall behaviour. Bphen and the Novaled materials give the best efficiencies, reaching up to 4 and 7 % respectively after stabilization. This in contrast to TPBi and PO-T2T which achieve neither high efficiencies nor long lifetimes. The peak emission wavelength of these devices shows a characteristic on a similar timescale as the efficiency stabilization. A gradual change happens over time until the emission stabilizes. Interestingly enough, the chosen ETL seems to have an influence on the stabilization rate and the stabilized emission wavelength which might indicate that the effect is likely interface related. The emission shifts towards 750 nm when using NET18 and almost 5 nm more towards 755 nm when Bphen is chosen as ETL. An overview of these results can be found in Table 3.3.

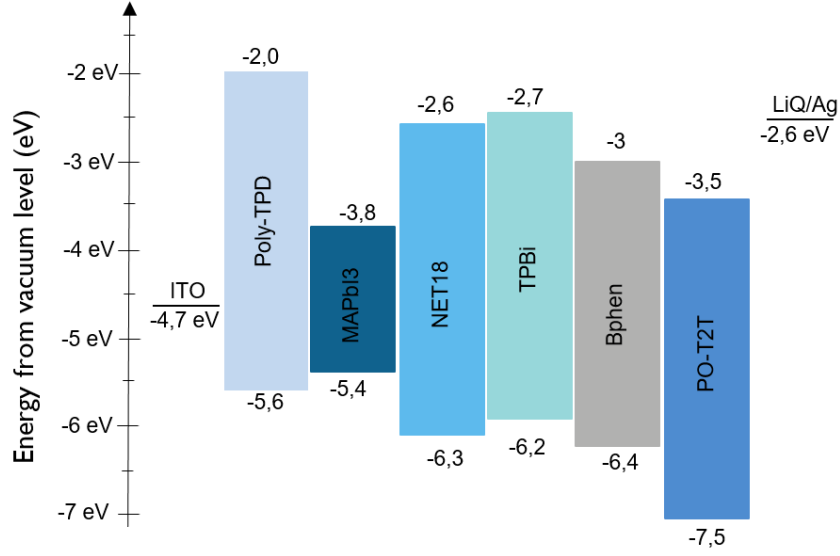


Figure 3.16: Bandalignment of the tested ETL materials together with the rest of the stack required to fabricate a PeLED.

Table 3.3: Overview of the device characteristics achieved with all the tested electron transport layers.

ETL/EIL/Metal Contact	average EQE (%)	max EQE (%)	Lifetime
TPBi/LiF/Al	0.768 ± 0.002	0.807 ± 0.004	160 seconds
PO - T2T/Liq/Ag	1.77 ± 0.01	2.25 ± 0.01	300 seconds
Bphen/Liq/Ag	5.011 ± 0.002	6.356 ± 0.009	> 2 Hours
NET18/doped NET18/Ag	6.58 ± 0.01	10.48 ± 0.02	T90 of 3.5 Hours

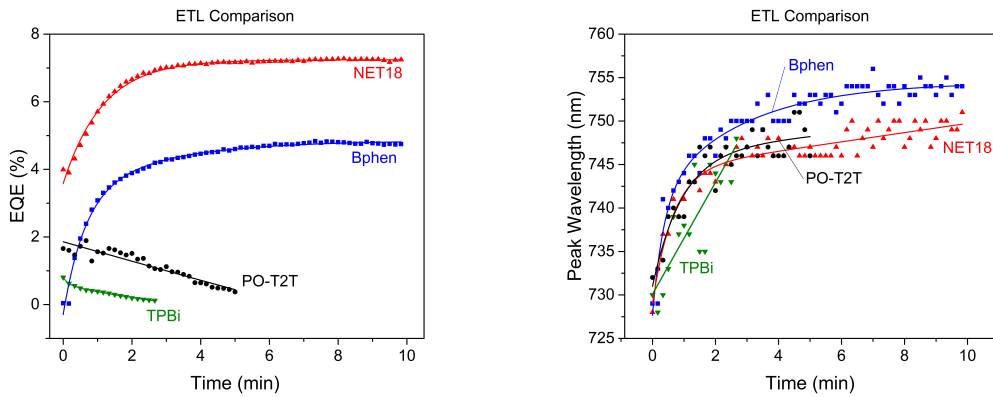


Figure 3.17: A comparison between ETLs and their typical devices characteristics. For each dataset a guide to the eye has been plotted to visualize its behaviour. left) The EQE values of various ETL layers over time. Bphen and NET18 results in high efficiencies after stabilization, while TPBi and PO-T2T remain below 2%. right) Tracking of the emission wavelength during the EQE measurement. The peak emission wavelength gradually shifts towards a slightly higher stabilized value.

3.3 Emission zone

Further improvements in the performance can be made by learning where the emission zone is situated in the device and tuning the optical cavity to suite it better. Locating it was done by stepwise changing the EIL thickness which allows to indirectly determine its position since it tunes the light emitting cavity and the intensity of the local electromagnetic field inside. [38] Afterwards the position of the emission zone could be found by comparing the measured EQE values and electromagnetic field simulations. For this purpose the Novald transport materials are used since they offer the best efficiency and allow the usage of thicker layers while still maintain good electrical properties.

Figure 3.18 left) shows two schematics of the method. Since the emission wavelength of the light is 750 nm the electromagnetic field inside the device has a wavelength of λ/n . For this specific perovskite the refractive index n is equal to 2.12 at 750 nm, in general organic materials also have a refractive index around 2 thus for the schematic the refractive index of perovskite is used for the whole cavity. Half of the wavelength of the medium is than about 180 nm. To see what kind of device efficiency has to be expected the wave is plotted on top of the LED stack. In the top schematic or the optimal case, the peak of the electromagnetic field coincides nicely with the emissive layer. On the other hand, in the bottom schematic the electromagnetic field almost has no overlap with the emissive layer.

In reality the EIL thickness was varied from the standard 20 nm up to 180 nm in steps of 40 nm while the ETL was held constant at 20 nm. At each point several devices were measured after stabilization, their datapoints can be seen in Figure 3.18 right). The EQE changes with the ETL thickness due to the cavity in the LED becoming larger. Since the light emitting zone stays in place this causes the emission to occur at unfavorable places in the cavity according to the electromagnetic field. A dip in EQE can be seen when the overlap between the electromagnetic field and the emissive layer is minimal. After which which the second maximum of the electromagnetic field overlaps more with the emissive layer increasing the EQE again.

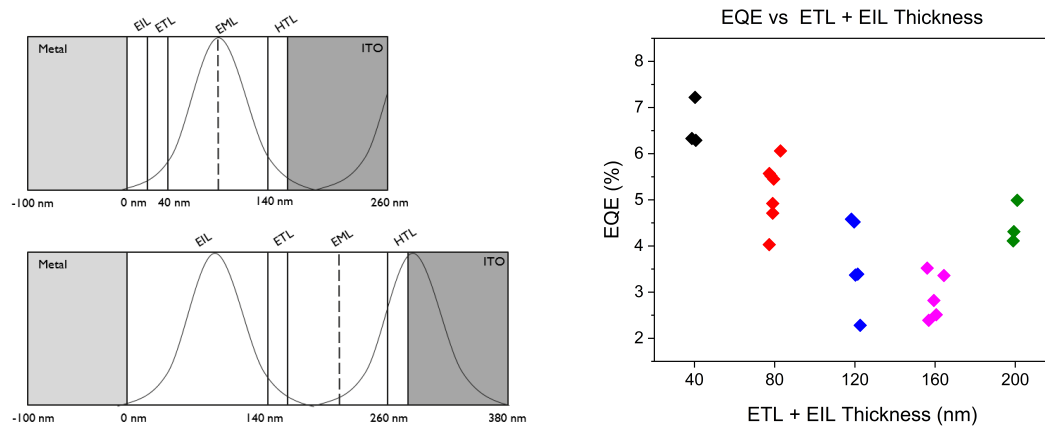


Figure 3.18: left) Two schematics of LED stacks together with electromagnetic field expected inside. The overlap of the emission zone and electromagnetic field can be changed by tuning the individual layer thickness. The schematic for the highest and lowest achieved efficiencies with the experimental stacks are shown here. right) EQE data after stabilization from the devices having different EIL thicknesses.

The next part in finding the emission zone in the device is matching the experimental data with simulations of the electromagnetic field. These simulations were performed by using the trans-

fer matrix algorithm. Parameters that could be changed in the simulation were the emission wavelength, the emission zone width and the position of the emission zone from the ETL. A script was made to seek the best match between the measured data and the parameters in the simulation.

Figure 3.19 left) shows how the simulation was approached concerning the start of the emission zone and the emission zone itself. The start was tuned from 0 to 90 nm, while the width was tuned from 100 to 10 nm. Figure 3.19 right) shows the simulated LED behaviour for an emission zone of 50 nm wide at various starting positions. The best match of the experimental and simulated data occurs when the emission zone starts at the edge of the ETL. This indicates that the hole mobility of the perovskite is much higher than the electron mobility.

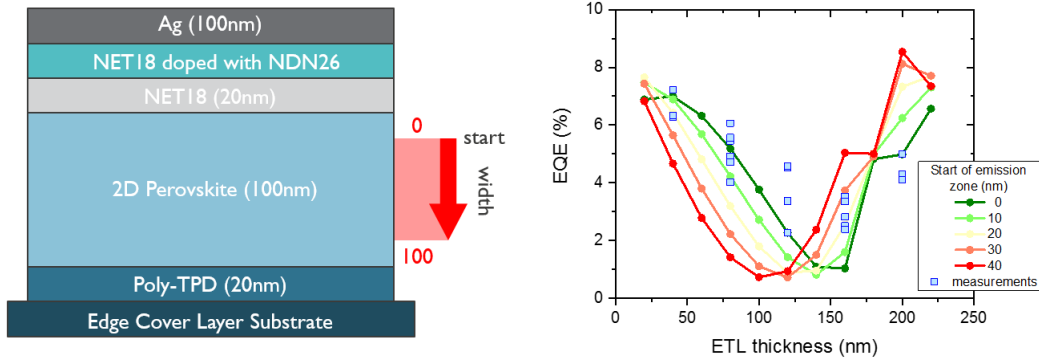


Figure 3.19: left) Schematic of the simulation and the employed parameters. right) Combination of the experimental and simulated data points. The emission zone was always taken as 50 nm wide in the plotted simulations

3.4 Peak Shift and prevention

3.4.1 Emission Peak Shift

An interesting effect that can be observed in PeLEDs is that the emission wavelength gradually shifts towards a stabilized emission. Typical peak shift behaviour can be seen in Figure 3.20 a) where over the course of 10 minutes the emission of the device gradually shifts to be centered around 750 nm. After each measurement the device was given 10 minutes to relax to its original state before starting a new measurement. The effect appears reversible since the emission onset starts at a similar wavelength each time. On top of that, it occurs on a shorter timescale in each consecutive burn, indicating that the underlying mechanism speeds up. The accompanying EQE data is shown in Figure 3.20 b) which shows that each consecutive burn degrades the device by about 1%. Hence the process does not seem completely reversible. A possible explanation is the formation of nonradiative traps during the relaxation of the device.

Since both 2D and 3D PeLEDs show this behaviour it is not related to the dimensionality of the perovskite, other possible explanations include temperature related bandgap changes, ionic movement, emission zone movement and phase separation. The temperature related effects would occur if joule heating of the device would be severe enough to change the bandgap. To test this hypothesis a sample was heated on a hotplate after which it was quickly transferred to the measurement setup next to it. Figure 3.21 shows the emission onset. However, no substantial change can be seen between the spectra as the temperature does not appear to influence the bandgap enough to cause a difference.

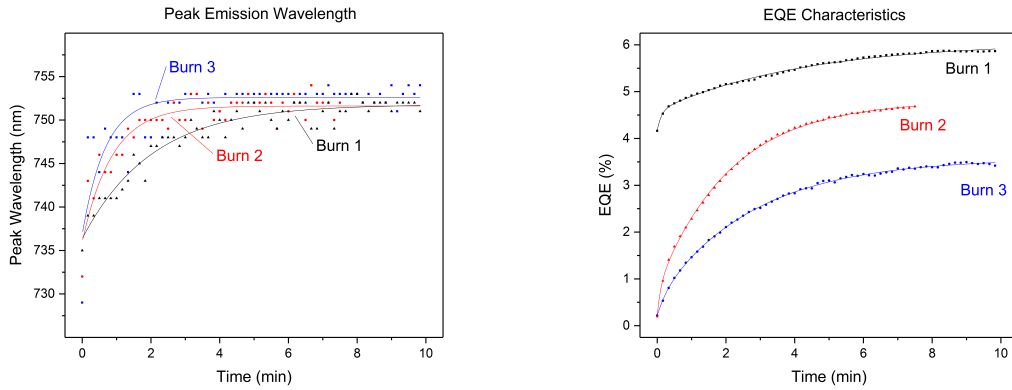


Figure 3.20: left) The emission shift through time of the same PeLED, between each measurement 10 minutes downtime was given to let the device relax to its initial position. A guide to the eye indicate the behaviour of the datapoints. right) The EQE through time behaviour of the same PeLED, again a guide to the eye visualizes the trend the datapoints follow. The device loses about 1% efficiency between each time it is turned on.

Ionic movement has already been observed in PSCs and thus very well could also be a factor in PeLEDs, especially since mixed halide perovskites are used. Slight differences between the diffusion coefficients of each halide could lead to an accumulation or depletion of a certain type of halide changing the material's bandgap. Alternatively, the accumulation could very well happen at the interfaces since PSCs were found to have some intrinsic capacitance likely causing the anomalous hysteresis. Possible consequences could be improved charge injection changing the balance of the ambipolar current. This would cause the emission zone to move possibly making the outcoupling for a different wavelength better. Finally, ionic movement has also shown to cause a phase separation in mixed halide perovskites where some of the new phases have a slightly lower bandgap and could act as charge trap and emission center.

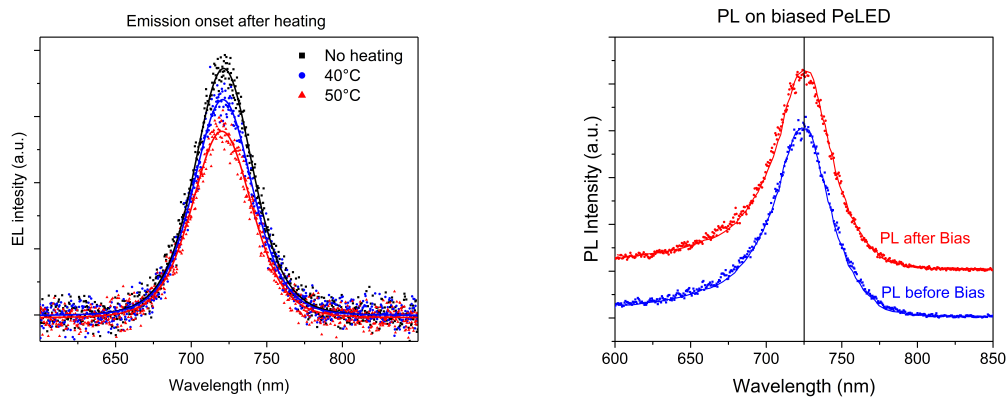


Figure 3.21: left) Electroluminescence onset spectra of a heated PeLED which shows no significant difference in emission wavelength indicating that the peak shift is likely not temperature related. A guide to the eye is plotted to better reflect the trend of the datapoints. right) PL spectra before and after a PeLED was biased. They were slightly offset to better illustrate that there is no difference between them. A guide to the eye has been plotted to better represent the behaviour of the data.

In the case of a phase separation the photoluminescence spectrum of a device should change before and right after a PeLED was biased. PeLEDs were mounted in an nitrogen atmosphere encapsulation box to avoid degradation in air, a quartz window allows the laser to probe the sample and build in contacts can bias the devices. After the initial PL measurement the devices were biased until the emission shift stabilized after which they were quickly measured again. The PL measurements in Figure 3.21 left) show no noticeable difference between the two situations. A possible explanation is that the ionic accumulation is very localized so the PL measurement cannot observe it. The aforementioned islands that possibly form in a phase separation could be small enough to almost immediately return the perovskite to its initial well mixed state. In any case, this measurement strongly disagrees with the entire emission zone undergoing a large phase separation. Another interesting thing to note is that the PL spectra did not get brighter, hence there is no reduction of nonradiative pathways hence there is no cleaning of traps that has been observed in PSCs. [30]

3.4.2 Efficiency Increase

Next to the emission shift there is also a change in the external quantum efficiency during operation. Figure 3.22 shows the behaviour of typical devices whose efficiency increases over the course of a few minutes after which it stabilizes. Comparing the emission onset with the stabilized emission shows that the efficiency increases to about its double. All in all this effect seems very similar to the emission peak shift and occurs on a similar timescale.

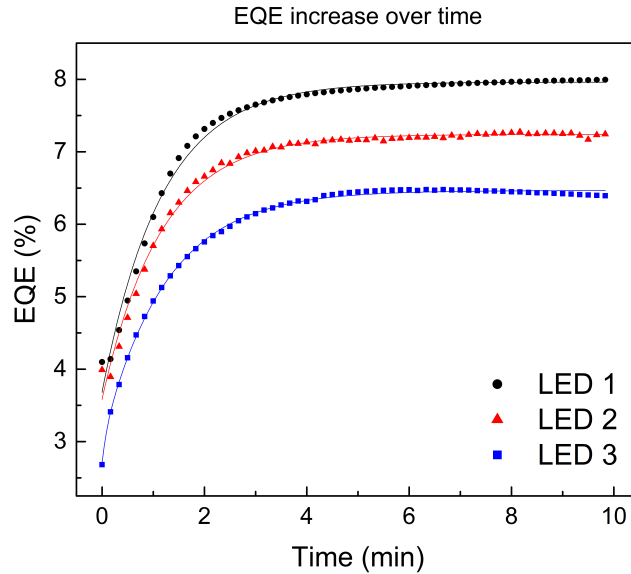


Figure 3.22: Typical increase in efficiency during device operation. Immediately after a device is turned on its efficiency start to gradually increase until it reaches a stabilized value. The increase is possibly related to moving iodide ions in the emissive layer. A guide to the eye has been plotted in the graph to better show the trend of the data. The error bars have not been plotted as they are smaller than the symbols for each datapoint.

Plausible explanations are that ion migration causes the emission zone to move or that the perovskite itself undergoes changes making light emission more efficient. If the emission zone were to move it could be related to the injection of charge carriers becoming more efficient. This

could be an interface effect caused by some ion accumulation at the edge. Alternatively the effect could be caused by ionic accumulation in the emission zone causing some form of phase separation which could be a direct consequence of the use of mixed halide perovskites. A light induced phase separation has already been observed in PSCs which causes islands to form having either a higher bromide or iodide concentration. The iodide rich islands have a lower bandgap and reduce the open circuit voltage. In the case of a PeLED these islands can act as a carrier trap and become the main emission centers which could have more efficient charge recombination and thus lead to higher EQE values. Another approach is that the increase in efficiency is related to the capacitance often observed in PSCs. In this scenario the diode and capacitor would share the applied current since they act in parallel as can be seen in Figure 3.23 left). As soon as the LED is forward biased the capacitor would start charging up and thus draining the current actually meant for the LED. The LED is thus not really less efficient, it receives less current than it is supposed to due to the capacitor. However as the capacitor charges less current flows through it and more current starts flowing through the device. When the capacitor is fully charged it no longer plays a role in the device characteristics. Interestingly to note is that the current charging a capacitor follows an exponential decay, thus the current flowing through the device would increase inversely, matching well with the experimental observations. Figure 3.23 right) is a schematic that shows the behaviour of both currents right after the device is turned on. In this case the term efficiency increase is a bad choice of words, as the effect is caused by an increasing diode current and the LED might not increase its actual efficiency at all. This would also lead to an adjustment of the previously mentioned lifetimes of the devices. Instead of having to wait for a device to burn in all datapoints of the lifetime measurements could contribute. By factoring in that the diode receives less current it is possible to extract the actual current flowing through the diode and thus also the actual EQE.

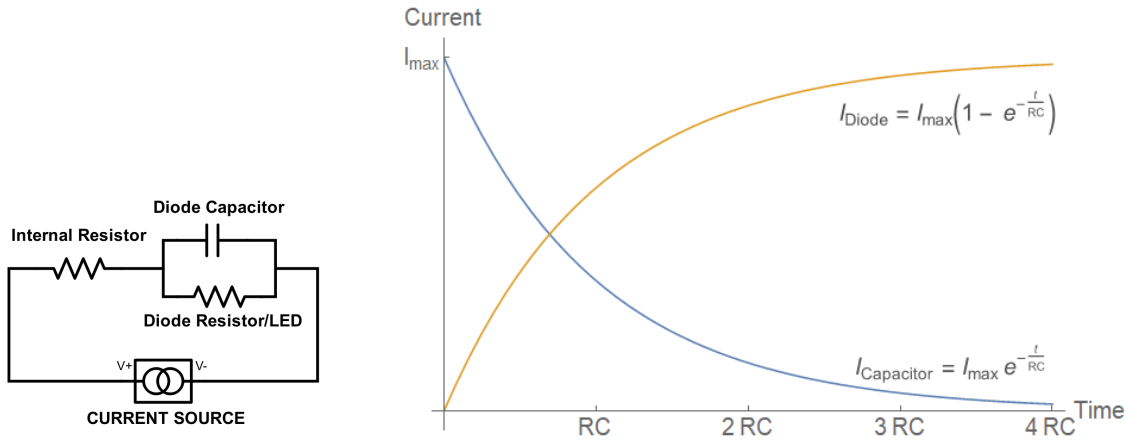


Figure 3.23: left) Schematic of the circuit that could lead to the observed effects. right) Schematic of the behaviour of the currents in a PeLED if it also has some capacitance due to ionic accumulation. The increasing diode current might explain what is observed as an increase in efficiency.

3.4.3 Preventing Ion movement

Since the main suspect causing the emission shift was ion migration, a method to freeze the ions in place was sought. Impedance spectroscopy measurements on PSCs have shown that there is a large capacitance at low frequencies. [34] However, at sufficiently high frequencies it is barely noticeable. Hence a possible solution to the ion migration is driving a device with a pulse at the right frequency. To test this hypothesis, pulsed driving was initially tested at 20 Hz with pulses of varying height. Various negative voltages were used as base from which the positive pulse always

went to 4.5V. Additionally, the negative part of the pulse was applied 4 times longer in an attempt to balance ion movement going in both directions. However, these measurements still showed a shift in emission wavelength albeit slowed down from normal biasing conditions. In a second attempt the frequency was raised to 5 kHz, the positive pulse still went to 4.5V while the negative pulse went to -0.5V. The base of the measurement could not be chosen as a negative voltage so there were two peaks with some downtime between them each returning to 0 V. Figure 3.24 shows the data as well as how a pulse at 20 Hz looked like. To better compare the data points with a normal constant bias, the time was adjusted to the time that the device was forward biased.

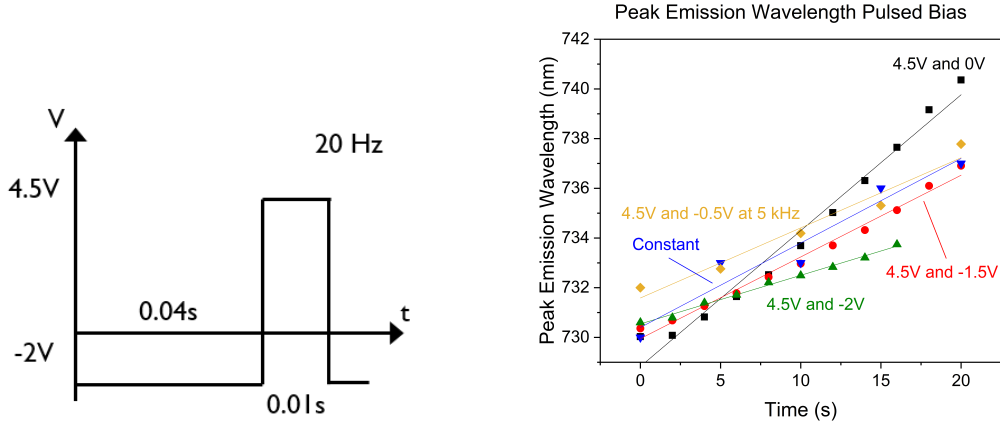


Figure 3.24: left) Schematic of a how the 20 Hz pulses looked like. right) Comparison between pulsed and steady state device characteristics. Pulsed measurements show some promise in slowing down the emission peak shift but also damage the devices faster.

When comparing the emission shift between the 20 Hz pulses and a constant current the pulses do appear to slow down the emission shift. Moreover, the more negative the negative part of the pulse is, the smaller the emission shift is. A downside of this method is that the device cannot endure these negative pulses for long periods of time as its reverse breakdown voltage is quite low. This is also the reason why the -2V data has less datapoints than the others, already after 15 seconds of uptime the device degraded. The higher frequency pulses at 5 kHz also showed a peak shift which is likely caused by the fact that the positive and negative part of the pulse were not properly balanced. Some further measurements and experiments where the pulses are varied might be necessary to gain some more insight if this could be a solution to the problem.

Chapter 4

Summary, Conclusions and Outlook

Perovskite based light emitting diodes were manufactured by a two-step spincoating technique resulting in highly efficient and stable device operation. Initially the devices suffered from severe degradation immediately after bias was turned on, leading to a typical lifetime of several minutes. Quasi 2D perovskites were chosen as possible solution to this problem as they intrinsically confine the charge carriers in the perovskite by forming quantum well-like structures. As a consequence the exciton binding energy of the material increases which in turn causes the excitons themselves to become more stable giving them the time to recombine radiatively. Careful tuning of the precursor solutions allowed to find an optimal spot between conduction and confinement. Subsequently, the device stack itself was improved by finding the most suitable ETL and optimal layer thicknesses. In the end devices such as shown in Figure 4.1 with an EQE of over 10% and a T90 of about 3.5 hours at 667 A/m² were achieved. These devices were made with precursor containing butylammonium iodide or BAI (C₄H₁₂IN) equal to 50 % of the molar concentration of PbI₂ in the solution.

Additionally, several experimental techniques were used to characterize the perovskites properties including photoluminescence, X-ray diffraction and scanning electron microscopy. PL measurements revealed that the perovskite film was quite nonuniform possibly due to poor mixing of the separate precursors during the spincoating or due to the solvents having different evaporation speeds. XRD showed that the quasi 2D film was almost not crystalline at all as only the slightest notion of the typical perovskite peaks could be found. Moreover, no peaks related to a 2D phase could be found. Instead it is possible that there are extremely small perovskite crystallites in a more micellar-like structure with a high degree of disorder. The SEM and optical microscopy measurements showed that the film was covered with pinholes at its surface.

Finally the device characteristics were looked into. Several interesting effects could be found in a standard device as it showed an efficiency increase and a shift in its emission wavelength, possibly related to each other. The efficiency increase is a possible consequence of the high capacitance perovskites show at low frequency biasing due to ionic movement. When a device is forward biased this capacitance will drain some of the applied current and the PeLED will seemingly have a low efficiency. After some time halide ions will have completely saturated the perovskite/ETL interface and the capacitance will become negligible. In turn all the applied current now flows through the LED and a higher efficiency is observed. Figure 3.23 shows how the behaviour of both the diode and capacitor current would look like through time if a capacitive effect were the root cause of the effect. The change in emission wavelength might be related to the same ionic accumulation as this might result in some amount of band bending at the interface, leading to better charge injection. This in turn might shift the emission zone in the LED enough so that the peak emission shifts with several nanometer. Alternatively, the emission shift can also be a

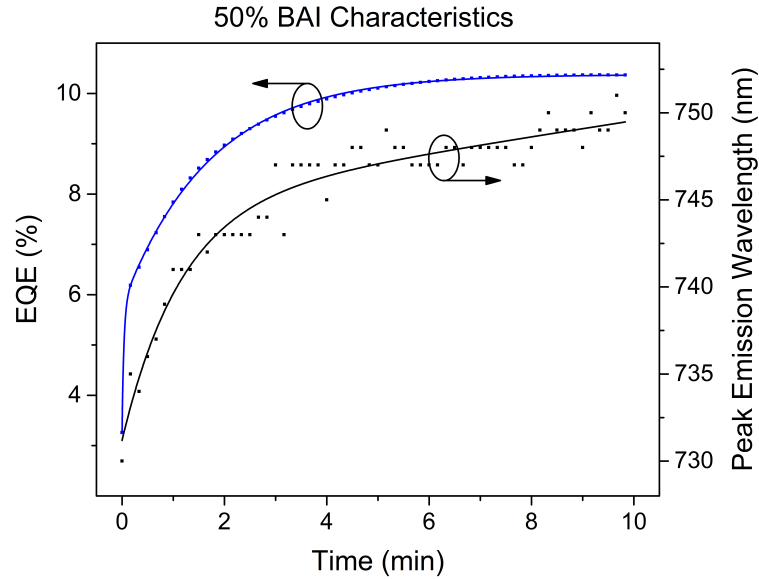


Figure 4.1: The device characteristics of the most optimal PeLED. The efficiency and emission wavelength increase gradually towards a stabilized value. These effects might be related to Ionic movement in the perovskite layer. A guide to the eye has been plotted to indicate the trend in the data. The error bars have been left out since they are not larger than the symbols indicating each point.

more direct consequence of the ion accumulation since a more iodide based perovskite leads to red shifted emission.

Perovskite materials show promise as light emitters as they are already reaching relatively high efficiencies given how new this research field is. However, more steps need to be taken to achieve efficiencies and lifetimes that can rival those of for example OLEDs. A good starting point would be research into the perovskites themselves and their device characteristics. Specifically ion migration and its possible side-effects such as a shift in emission wavelength and an increase in efficiency still need to be understood in detail. On top of their use in LEDs, amplified spontaneous emission has been observed in these materials which possibly opens a gateway towards lasing applications. The great strength of perovskites here would be that they are used as a thin film and thus could lead to a electrically pumped thin film laser which can be used on microchips for photonic communication. An first step in this direction could be light emitting transistors or LETs as they allow for a much higher current density to be used than in a regular LED. The main challenge here would be to properly balance the ambipolar charge transport in the perovskite.

Bibliography

- [1] T. Jeon et al. Hybrid perovskites: Effective crystal growth for optoelectronic applications. *Advanced Energy Materials*, 7(19):1602596, 2017. 2
- [2] G. W. P. Adhyaksa et al. Carrier diffusion lengths in hybrid perovskites: Processing, composition, aging, and surface passivation effects. *Chemistry of Materials*, 28:5259–5263, 2016. 3
- [3] Z.K. Tan et al. Bright light-emitting diodes based on organometal halide perovskite. *Nature nanotechnology*, 9:687–692, 2014. 3
- [4] W. Zou et al. Minimising efficiency roll-off in high-brightness perovskite light-emitting diodes. *Nature Communications*, 9, 2018. 3, 7
- [5] S. Yakunin et al. Low-threshold amplified spontaneous emission and lasing from colloidal nanocrystals of caesium lead halide perovskites. *Nature Communications*, 6, 2015. 3
- [6] Y. Jia et al. Diode-pumped organo-lead halide perovskite lasing in a metal-clad distributed feedback resonator. *Nano Letters*, 16:4624–4629, 2016. 3
- [7] M.A. Becker et al. Bright triplet excitons in caesium lead halide perovskites. *Nature*, 553:189–193, 2018. 4
- [8] Y.H. Kim et al. Metal halide perovskite light emitters. *PNAS*, 113(42):11694–11702, 2016. 4
- [9] T.H. Han et al. Molecularly controlled interfacial layer strategy toward highly efficient simple-structured organic light-emitting diodes. *Advanced Materials*, 24(11):1487–1493, 2012. 4
- [10] D. Kabra et al. Efficient single-layer polymer light-emitting diodes. *Advanced Materials*, 22(29):3194–3198, 2010. 4
- [11] B. Mashford et al. High-efficiency quantum-dot light-emitting devices with enhanced charge injection. *Nature Photonics*, 7:407–412, 2013. 4
- [12] X. Dai et al. Solution-processed, high-performance light-emitting diodes based on quantum dots. *Nature*, 515:96–99, 2014. 4
- [13] M. Era et al. Organic-inorganic heterostructure electroluminescent device using a layered perovskite semiconductor ($\text{C}_6\text{H}_5\text{C}_2\text{H}_4\text{NH}_3$) $_2\text{PbI}_4$. *Applied Physics Letter*, 65(6):676–678, 1994. 5
- [14] J. Wang et al. Interfacial control toward efficient and low-voltage perovskite light-emitting diodes. *Adv. Mater.*, 27:2311–2316, 2015. 6
- [15] A. Miyata et al. Direct measurement of the exciton binding energy and effective masses for charge carriers in organotinorganic tri-halide perovskites. *Nature Physics*, (11):582–587, 2015. 6

- [16] H. Cho et al. Overcoming the electroluminescence efficiency limitations of perovskite light-emitting diodes. *Science*, 350:1222–1225, 2015. 6
- [17] X. Yang et al. Efficient green light-emitting diodes based on quasi-two-dimensional composition and phase engineered perovskite with surface passivation. *Nature Communications*, 9:1–8, 2018. 7, 14
- [18] H. Nakanotani et al. High-efficiency organic light-emitting diodes with fluorescent emitters. *Nature Communications*, 5, 2014. 7
- [19] R. Meerheim et al. High-efficiency monochrome organic light emitting diodes employing enhanced microcavities. *Applied Physics Letters*, 93, 2008. 7
- [20] D. Tanaka et al. Ultra high efficiency green organic light-emitting devices. *Japanese Journal of Applied Physics*, 46, 2007. 7
- [21] R. Meerheim et al. Ultrastable and efficient red organic light emitting diodes with doped transport layers. *Applied Physics Letters*, 89,, 2006. 7
- [22] C. Eames et al. Ionic transport in hybrid lead iodide perovskite solar cells. *Nature Communications*, 6, 2015. 7, 9
- [23] J. M. Azpirov et al. Defect migration in methylammonium lead iodide and its role in perovskite solar cell operations. *Energy Environmental Science*, 8:2118–2127, 2015. 7
- [24] J. Haruyama et al. First-principles study of ion diffusion in perovskite solar cell sensitizers. *Journal of the American Chemical Society*, 137:10048–10051, 2015. 7
- [25] T. Yang et al. The significance of ion conduction in a hybrid organiceinorganic lead-iodide-based perovskite photosensitizer. *Angewandte Chemie*, 127:1–7, 2015. 8
- [26] A. Senocrate et al. The nature of ion conduction in methylammonium lead iodide : A multimethod approach. *Angewandte Chemie: International Edition*, 56:7755–7759, 2017. 8
- [27] C. Li et al. Real-time observation of iodide ion migration in methylammonium lead halide perovskites. *Small*, 13, 2017. 8, 10
- [28] E. T. Hoke et al. Reversible photo-induced trap formation in mixed-halide hybrid perovskites for photovoltaics. *Chemical Science*, 6:613–617, 2015. 9
- [29] C. G. Bischak et al. Origin of reversible photoinduced phase separation in hybrid perovskites. *Nano Letters*, 17:1028–1033, 2017. 10
- [30] D.W. deQuilettes et al. Photo-induced halide redistribution in organiceinorganic perovskite films. *Nature Communications*, 7, 2016. 10, 38
- [31] Z. Xiao et al. Mixed-halide perovskites with stabilized bandgaps. *Nano letters*, 17:6863–6869, 2017. 11
- [32] H. J. Snaith et al. Anomalous hysteresis in perovskite solar cells. *Physical Chemistry Letters*, 5:1511–1515, 2014. 11, 12
- [33] S. Ravishankar et al. Surface polarization model for the dynamic hysteresis of perovskite solar cells. *Journal of Physical Chemistry Letters*, 8:915–921, 2017. 12
- [34] B. Chen et al. Impact of capacitive effect and ion migration on the hysteretic behavior of perovskite solar cells. *Physical Chemistry Letters*, 6:4693–4700, 2015. 12, 39
- [35] C. Li et al. Iodine migration and its effect on hysteresis in perovskite solar cells. *Advanced Materials*, 28:2446–2454, 2016. 12

- [36] L. Zhao et al. Electrical stress influences the efficiency of $\text{CH}_3\text{NH}_3\text{PbI}_3$ perovskite light emitting devices. *Advanced Materials*, 29, 2017. 13, 14
- [37] Y. Zou et al. Temperature-dependent bias poling and hysteresis in planar organometal halide perovskite photovoltaic cells. *Advanced Energy Materials*, 6, 2016. 13
- [38] M. Furno et al. Efficiency and rate of spontaneous emission in organic electroluminescent devices. *Physical Review B*, 85, 2012. 35

Acknowledgments

I would like to start by thanking the Eindhoven University of Technology for allowing me to pursue the opportunity to do my masterthesis at IMEC. Secondly, a special thanks goes to prof. R. Coehoorn for supporting me along the way during our regular meetings giving feedback and shedding light onto details that needed further exploring. Additionally, I would like to thank all the committee members for taking the time to read and evaluate this thesis.

Of course, I cannot forget IMEC, the LAE departemnt and all its employees for giving me a warm welcome and all the help I received during my stay. However, several people deserve some more credit. A special thanks goes to dr. W. Qiu who mentored me and provided valuable feedback. Next, I would like to thank dr. R. Gehlhaar for his insights and guidance. Another special thanks goes to prof. J. Genoe for his insights and giving me the opportunity to join the department. Finally I would like to extend a special thanks to Carolina, Dieter, Joana, Khalid, Mafalda and Robby for making my time at IMEC much more enjoyable.

Appendix A

Scanning Electron Microscopy

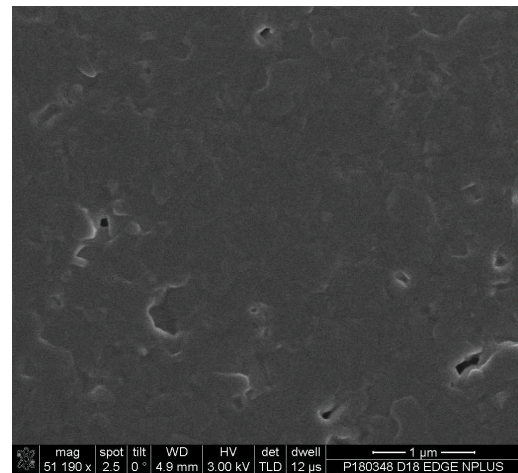
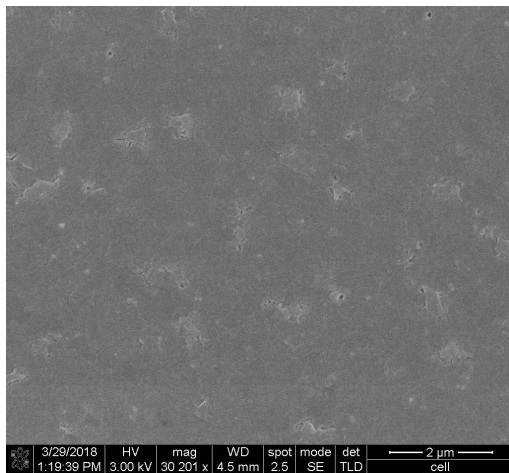


Figure A.1: Scanning electron microscopy images of 2D perovskite samples having 30% (left) and 70% (right) BAI.

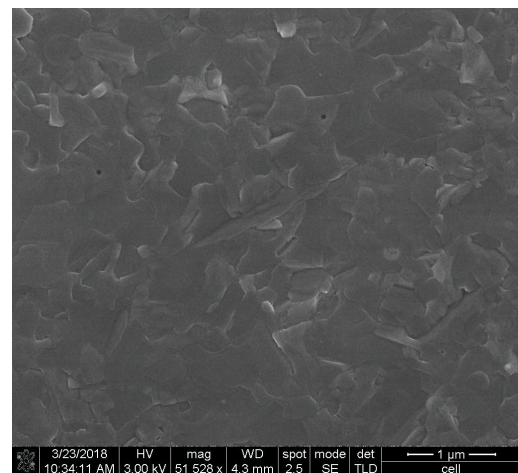
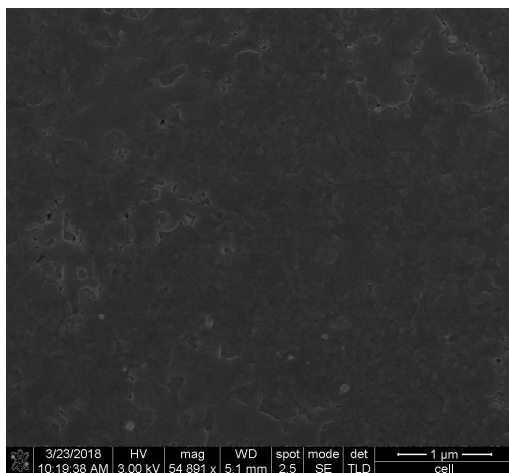


Figure A.2: Scanning electron microscopy images of 50% BAI 2D perovskite samples annealed at 60°C (left) and 100°C (right).